

Diffractive scattering

E.A. De Wolf†§

† CERN, European Laboratory for Particle Physics, 1211 Geneva 23, CH

Abstract. We discuss basic concepts and properties of diffractive phenomena in soft hadron collisions and in deep-inelastic scattering at low Bjorken- x . The paper is not a review of the rapidly developing field but presents an attempt to show in simple terms the close inter-relationship between the dynamics of high-energy hadronic and deep-inelastic diffraction. Using the saturation model of Golec-Biernat and Wüsthoff as an example, a simple explanation of geometrical scaling is presented. The relation between the QCD anomalous multiplicity dimension and the Pomeron intercept is discussed.

1. Introduction

After nearly two decades outside of the mainstream of high-energy physics, the subject of diffractive scattering has made a spectacular come-back with the observation of Large Rapidity Gap events at the HERA ep collider and similar studies at the highest energy hadron colliders. It has become a field of intense research and many detailed aspects have been repeatedly reviewed [1, 2].

To develop a phenomenology of very high energy scattering and diffraction, a field of research which originated in soft hadron hadron collisions, it is tempting and traditional to start from a t -channel formalism based on Regge theory. For deep-inelastic scattering (DIS) and hard diffractive processes this leads to the simple (and popular) Pomeron picture as first proposed by Ingelman and Schlein [3]. Although Regge theory is perfectly valid and beautiful, based on very general properties of the scattering amplitudes, it is plagued by many problems in practical applications which, as happened in the past, severely limit its predictive power. Apart from the fundamental theoretical question how to derive the theory as a strong-coupling limit of QCD, the theory itself provides little insight into the relation between properties of the final states, the structure of the theory and the physical meaning of its parameters. This becomes particularly important when the formalism is used outside its traditional domain of application, such as in deep-inelastic scattering.

In this paper, we shall mainly adopt an s -channel picture of diffraction. Diffractive scattering is explained by the differential absorption by the target of the large number

§ Also at University of Antwerpen, Physics Department, Universiteitsplein 1, B-2610 Antwerpen, Belgium (eddi.dewolf@ua.ac.be)

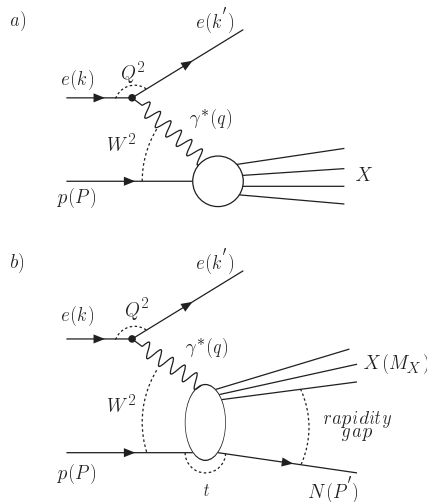


Figure 1. Kinematic variables (a) for the reaction $e p \rightarrow e X$; (b) for the semi-inclusive reaction $e p \rightarrow e N X$ with a rapidity gap.

of states which coherently build up the initial-state hadron or (virtual) photon and scatter with different cross sections. Such an approach incorporates from the outset basic quantum mechanics and unitarity, and permits, at least conceptually, a unified treatment of hadron, and real and virtual photon scattering. It will allow us to appreciate the close inter-relation between the dynamics of high-energy hadronic and deep-inelastic diffraction (DDIS) at very small Bjorken- x and to understand that long-distance physics plays a very important role in both. It is also the approach used in the most successful of the present theoretical models [2].

The main thrust of the paper will be to argue that the physics can be understood on the basis of a surprisingly small number of dynamical ingredients. This in turn leads to a view of the collision dynamics which is simple enough to help develop intuition, provide physical insight and suggest fruitful avenues of research. The paper is mainly addressed to experimentalists entering the field and we hope it will broaden their view of the subject. No originality is claimed in the presentation of the material although any errors of interpretation should be attributed solely to the author.

2. Preliminaries

2.1. DIS kinematics and cross sections

The standard kinematical variables to describe ep DIS are depicted in figure 1a. The centre-of-mass energy squared of the ep system is $s = (P + k)^2$, with P and k the initial-state four-momenta of the proton and electron (or positron), respectively. W , the CMS energy of the virtual-photon proton system, is given by $W^2 = (P + q)^2$. The photon

virtuality Q^2 and the Bjorken variables x and y are defined as

$$q^2 = -Q^2 = (k - k')^2, \quad x = \frac{Q^2}{2P \cdot q} = \frac{Q^2}{W^2 + Q^2 - m_p^2}, \quad y = \frac{P \cdot q}{P \cdot k}. \quad (1)$$

Neglecting the proton mass, one has

$$Q^2 = x y s, \quad W^2 = Q^2 \frac{1-x}{x} \simeq \frac{Q^2}{x}, \quad (2)$$

the latter expression being valid for $x \ll 1$.

For the ‘‘rapidity-gap’’ process presented in figure 1b, and where a baryon with four-momentum P' is detected in the final state, one defines the additional variables

$$t = (P - P')^2; \quad \xi = \frac{Q^2 + M_X^2 - t}{Q^2 + W^2}; \quad \beta = \frac{Q^2}{Q^2 + M_X^2 - t} = \frac{x}{\xi}, \quad (3)$$

The variable ξ is the fractional energy-loss suffered by the incident proton. The variable β can naively be thought of as representing the fractional momentum carried by a struck parton in an object—Pomeron or Reggeon—carrying longitudinal momentum ξ , emitted by the proton and subsequently undergoing a hard scatter. For small $|t|$ one has

$$\beta = \frac{Q^2}{Q^2 + M_X^2} = \frac{x}{\xi}; \quad M_X^2 = \frac{1-\beta}{\beta} Q^2; \quad \xi = \frac{(Q^2 + M_X^2)}{W^2}. \quad (4)$$

In strict analogy with the total ep cross section

$$\frac{d^2\sigma}{dx dQ^2} = \frac{4\pi\alpha_{em}^2}{x Q^4} \left[1 - y + \frac{y^2}{2(1+R)} \right] F_2(x, Q^2), \quad (5)$$

which defines the structure function $F_2(x, Q^2)$ (α_{em} is the QED coupling), the differential cross section for a semi-inclusive (SI) DIS process (figure 1b) can be written as

$$\frac{d^3\sigma}{dx dQ^2 d\xi} = \frac{4\pi\alpha_{em}^2}{x Q^4} \left[1 - y + \frac{y^2}{2(1+R)} \right] F_2^{SI(3)}(\xi, x, Q^2). \quad (6)$$

Alternatively, in measurements of the diffractive ($D(3)$) contribution to $F_2(x, Q^2)$, one often uses the definition

$$\frac{d^3\sigma}{d\beta dQ^2 d\xi} = \frac{4\pi\alpha_{em}^2}{\beta Q^4} \left[1 - y + \frac{y^2}{2(1+R)} \right] F_2^{D(3)}(\xi, \beta, Q^2), \quad (7)$$

replacing x by β in equation (6). $R = \sigma_L/\sigma_T$ is the ratio of the cross sections for longitudinally and transversely polarized virtual photons. Since y is usually small in experiment, R can be neglected. Equations (6) and (7) are equivalent since they represent the same experimental data. From an experimental point of view, there is no a priori reason to prefer one over the other and both should be measured. For fixed (x, Q^2) (i.e. W fixed), the ξ dependence of $F_2^{SI(3)}(\xi, x, Q^2)$ reflects that on M_X . Alternatively, for fixed (β, Q^2) (i.e. M_X fixed) the W dependence of $F_2^{D(3)}(\xi, \beta, Q^2)$ is explored by varying ξ .

The structure function F_2 is related to the absorption cross section of a virtual photon by the proton, σ_{γ^*p} . For diffractive scattering at high W (low x), we have similarly

$$F_2^{D,SI(3)}(x, Q^2, \xi) = \frac{Q^2}{4\pi^2\alpha_{em}} \frac{d^2\sigma_{\gamma^*p}^{D,SI(3)}}{d\xi dt}. \quad (8)$$

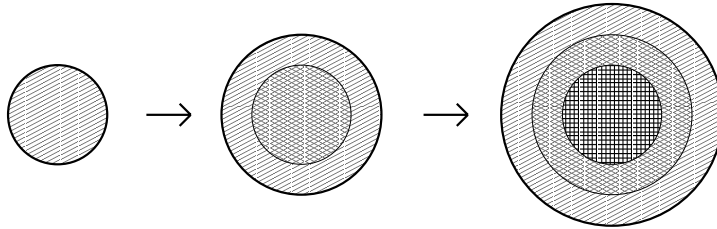


Figure 2. Qualitative picture of the high-energy evolution of a hadronic target in impact parameter space. From [4].

2.2. Regge formalism

2.2.1. Total and elastic cross sections. Since the Regge formalism is so often used in present analyses of diffractive HERA data, it is useful to recall here its main ingredients and predictions. For small-angle elastic scattering of two hadrons a and b at high s , dominated by Pomeron exchange, the Regge scattering amplitude (ignoring the small real part) takes the factorized form

$$\mathcal{A}_{el}^{ab}(s, t) = is\beta_a(t)(s/s_0)^{\alpha_{\mathcal{P}}(t)-1}\beta_b(t). \quad (9)$$

Here, s_0 is an arbitrary mass scale, frequently chosen to be of the order of 1 GeV². The dependence on the species of the incoming hadron is contained in the form factors, $\beta_{a,b}(t)$, usually parameterized as an exponential $\propto \exp(B_{0;a,b}t)$. $\alpha_{\mathcal{P}}(t)$ is the Pomeron trajectory. In its simplest version it is a Regge pole, with intercept $\alpha_{\mathcal{P}}(0) = 1 + \epsilon$, slightly larger than 1; ϵ controls the large- s or large W growth of the total and elastic cross sections. The name ‘‘Pomeron’’ was first used in [5], but first discussed by V.N. Gribov [6] and later named after Y. Pomeranchuk [7]. The observed large- s -dependence of the cross sections can be accommodated with a trajectory $\alpha_{\mathcal{P}}(t)$ of the form

$$\alpha_{\mathcal{P}}(t) = \alpha_{\mathcal{P}}(0) + \alpha'_{\mathcal{P}}t = 1 + \epsilon + \alpha'_{\mathcal{P}}t. \quad (10)$$

In Regge theory $\alpha_{\mathcal{P}}(t)$, i.e. $\alpha_{\mathcal{P}}(0)$ and $\alpha'_{\mathcal{P}}$, must be independent of the species of the particles colliding. We shall see that their meaning in terms of the particle production dynamics is, at least qualitatively, easy to understand. The energy dependences of the elastic and total cross section are given by

$$d\sigma_{el}^{ab}/dt|_{t=0} = \frac{1}{16\pi}[\beta_a(0)\beta_b(0)]^2(s/s_0)^{2\epsilon}, \quad (11)$$

$$\sigma_{\mathbb{T}}^{ab} = \beta_a(0)\beta_b(0)(s/s_0)^{\epsilon}. \quad (12)$$

The meaning of $\alpha'_{\mathcal{P}}$ becomes clear if one considers $d\sigma_{el}^{ab}/dt$ at small $|t|$, using an exponential approximation

$$d\sigma_{el}^{ab}/dt = \frac{1}{16\pi}[\beta_a(0)\beta_b(0)]^2 e^{B(s)t} (s/s_0)^{2\epsilon} = \frac{[\sigma_{\mathbb{T}}^{ab}]^2}{16\pi} e^{B(s)t}, \quad (13)$$

with

$$B(s) = 2 \left(B_{0;a} + B_{0;b} + \alpha'_{\mathcal{P}} \ln \frac{s}{s_0} \right). \quad (14)$$

The energy-independent terms $B_{0;a,b}$ originate from the form-factors in equation (9). From pp data $B_{0;p} \approx 2 - 3 \text{ GeV}^{-2}$.

Equation (14) shows that the forward elastic peak “shrinks” with energy: $B(s)$ increases (here logarithmically) with s . In impact parameter (\vec{b}) space (9) becomes

$$\mathcal{A}^{ab}(s, \vec{b}) = i \frac{\beta_a(0)\beta_b(0)}{8\pi} \frac{(s/s_0)^\epsilon}{B(s)} e^{-\vec{b}^2/2B(s)} \quad (15)$$

The transverse size of the “interaction region” is Gaussian with $B(s) = \langle \vec{b}^2 \rangle$.

The collision can be visualized in the impact-parameter plane, figure 2. The scattering profile is a disc with a b -dependent opacity, the mean radius of the disc being proportional to $\sqrt{B(s)}$. $B(s)$ contains an s -independent and a $\ln s/s_0$ term. The radius expands with s with a rate of growth determined by α'_P , estimated to be $\approx 0.25 \text{ GeV}^{-2}$ [8] (for a much earlier but similar estimate see [9]). At the same time, the opacity at fixed b is likely to increase too. In a perturbative QCD picture, this corresponds to an increase of the gluon density in the target or, in the proton rest frame, with an increase of the interaction probability (symbolized by increasing blackness in the figure). Since the latter cannot exceed unity, it follows that also the gluon density cannot rise indefinitely.

Concerning the meaning of $\alpha_P(0)$, it will become clear in section 6.2 that the increase of σ_T with s can be attributed to an increase of the number of (wee) partons in projectile and target. This will allow us to relate $\alpha_P(0)$ to the wee-parton density in rapidity or, more generally, to the QCD multiplicity anomalous dimension.

2.2.2. Triple-Regge parameterization of the reaction $a + b \rightarrow c + X$. Regge theory can be generalized to inclusive reactions. The invariant cross section of an inclusive process, $a + b \rightarrow c + X$, can be expressed in terms of the Regge-Mueller expansion which is based on Mueller’s generalized optical theorem [10]. This states that an inclusive reaction $ab \rightarrow cX$ is connected to the elastic (“forward”) three-body amplitude $A(ab\bar{c} \rightarrow ab\bar{c})$ via

$$E \frac{d^3\sigma}{dp^3}(ab \rightarrow cX) \sim \frac{1}{s} \text{Disc}_{M^2} A(ab\bar{c} \rightarrow ab\bar{c}), \quad (16)$$

where the discontinuity is taken across the M_X^2 cut of the elastic Reggeized amplitude. For the triple-Pomeron diagram, valid in the (diffractive) region of phase space where the momentum fraction of particle c is near one, or $s \gg W^2 \gg (M_X^2, Q^2) \gg (|t|, m_p^2)$, equation (16) has the approximate form

$$E \frac{d^3\sigma}{dp^3} = \frac{1}{\pi} \frac{d^2\sigma}{dt d\xi} \simeq \frac{s}{\pi} \frac{d^2\sigma}{dt dM_X^2} = f(\xi, t) \cdot \sigma_{\mathbb{P}p}(M_X^2), \quad (17)$$

where t is the four-momentum transfer squared. The “flux factor” $f(\xi, t)$ is given by

$$f(\xi, t) = N F^2(t) \xi^{[1-2\alpha_P(t)]}. \quad (18)$$

In the above equations, N is a normalization factor, $F(t)$ the form-factor of the $pp\mathbb{P}$ -vertex; $\sigma_{\mathbb{P}p}$ can be interpreted as the Pomeron-proton total cross section. Assuming $\sigma_{\mathbb{P}p} \sim (M_X^2)^\epsilon$, and using equation (10), (17) and (18) imply that

$$\left. \frac{d^2\sigma}{dt d\xi} \right|_{t=0} \sim \frac{s^\epsilon}{\xi^{(1+\epsilon)}} = \frac{(M_X^2)^\epsilon}{\xi^{(1+2\epsilon)}}. \quad (19)$$

The two expressions on the right-hand side equation (19) are equivalent. However, they show that the model predicts slightly different ξ dependences if either s is kept fixed and M_X varied, or if M_X^2 is fixed and s varied. Nevertheless, since ϵ is small, both expressions in equation (19) show that the triple-Regge $\mathbb{P}\mathbb{P}\mathbb{P}$ contribution in the region $\xi \ll 1$ is of the generic form

$$\left. \frac{d^2\sigma}{dt d\xi} \right|_{t=0} \sim \frac{1}{\xi^{(1+\delta)}} \quad \text{with } \delta \ll 1 \quad (20)$$

and predicts a “universal” $1/\xi$ dependence as long as δ is universal. Regge theory also implies that both σ_{el}/σ_T and σ^D/σ_T increase as s^ϵ . This eventually leads to violation of unitarity since ϵ is found to be positive. The total diffractive cross section, σ_T^D , grows as $s^{2\epsilon}$.

Although the applicability of Mueller’s optical theorem to reactions with (far) off-shell particles has not been proven, it is very frequently used as the starting point in analyses of diffractive phenomena in γ^*p scattering. In that case, s in the above equations has to be replaced by W^2 or $1/x$ if Q^2 is fixed.

2.2.3. Problems. In spite of the elegance of the Regge approach, it has been known for a long time [11] that the theory with a “super-critical Pomeron”: $\alpha_{\mathbb{P}}(0) = 1 + \epsilon$ ($\epsilon > 0$), is plagued by unitarity problems as $s \rightarrow \infty$ which are especially severe for inelastic diffraction: i) the power-law dependence, $\sigma_T \propto s^\epsilon$ violates the Froissart-Martin bound [12]; ii) the ratio $\sigma_{el}/\sigma_T \propto s^\epsilon/\ln s$ eventually exceeds the black-disk geometrical bound ($\sigma_{el} \leq \frac{1}{2}\sigma_T$); iii) the ratio σ_T^D/σ_T increases as s^ϵ . This disagrees with experiment not only for hadron collisions [13], but also for deep-inelastic diffraction, where the ratio σ_T^D/σ_T is found to be essentially independent of W [14, 15] (see section 4.3).

3. Experimental results on total and elastic cross sections

3.1. Energy dependence of hadronic total cross sections

The s -dependence of total hadron-hadron cross sections, σ_T , has been measured for many combinations of hadrons. Above ~ 20 GeV all hadronic cross sections rise with s . This was first discovered for K^+p collisions in 1970 at the Serpukhov accelerator [17]. The rise of the pp total cross section was first observed at the ISR [18] and later confirmed at Fermilab [19]. A compilation of $\bar{p}p$, pp and $\pi^\pm p$ data is shown in figure 3. The solid lines are fits which include a component decreasing rapidly with s and a second rising component which persists at high energies. In [16] it was observed that all measured

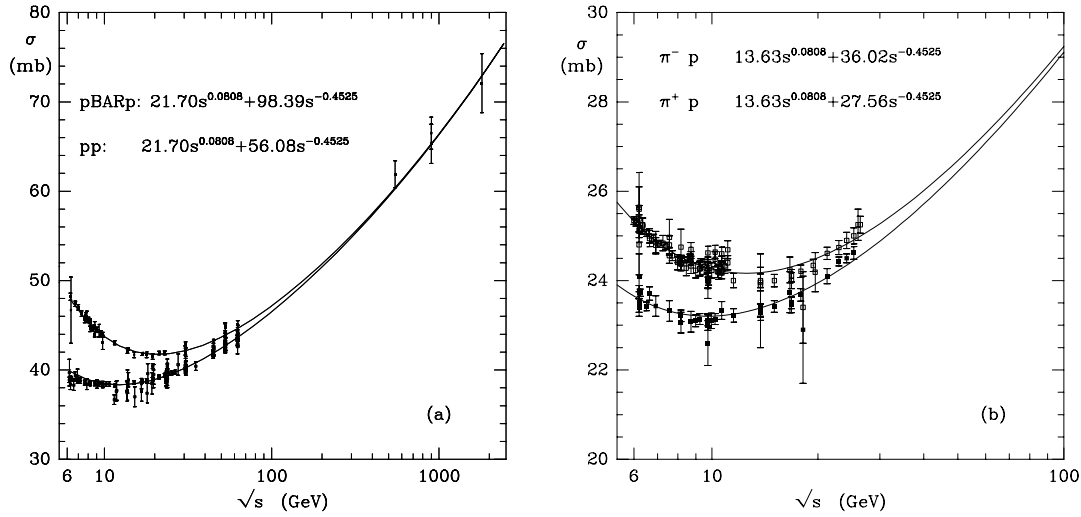


Figure 3. Total cross sections measured in hadronic scattering as a function of the centre-of-mass energy for pp , $p\bar{p}$, $\pi^\pm p$ scattering. The cross sections show a “universal” rise at high energies of the form $\sigma \sim s^{0.08}$ [16].

hadron-hadron (and γp) cross sections grow in an similar way at high s . An economical parameterization is a sum of two power-law terms in s

$$\sigma_T = X s^\epsilon + Y s^{\epsilon'}, \quad (21)$$

where the constants X and Y depend on the reaction. This obviously is inspired by Regge theory, the two terms in equation (21) corresponding to Pomeron and “normal” Regge (Reggeon) exchanges, respectively. The value of ϵ is not very precisely established. Various recent “global” fits find the data to be compatible with ϵ in the range $0.08 - 0.1$ [16, 20, 21]; ϵ' is found to be ~ -0.45 [16]. Global fits to total, elastic and diffractive cross sections performed much earlier yielded similar values for ϵ [22]. One should also note [23] that the present data cannot discriminate between “simple-pole” fits inspired by a Regge-model of t -channel exchanges leading to a power-law dependence, and equally valid fits to $\log^2 s$ and $\log s$ (or, for that matter, $e^{\sqrt{\log s}}$) functional dependences.

Although the significance of equation (21) has been over-emphasized, the “universal” high-energy behaviour of the total hadronic cross sections is an important observation which calls for deeper understanding. It also raises the question (not addressed in Regge theory) which particular final states are responsible for this increase.

As already mentioned, the single-Pomeron exchange amplitude violates unitarity thus indicating an inconsistency of this model. The simplest way of overcoming this problem without abandoning Regge theory altogether is the introduction of multiple Pomeron exchanges (or multiple interactions) in a single scattering process, as depicted in figure 4. The total amplitude can then be written as the sum of n -pomeron exchange amplitudes $A^{(n)}(s, t)$. For each n -pomeron graph one can define a theoretical “total”

cross section applying the optical theorem to the corresponding n -pomeron amplitude

$$\sigma^{(n)} = (-1)^{n+1} \frac{1}{s} \text{Im } m(A^{(n)}), \quad \sigma_{\text{tot}} = \sum_{n=1}^{\infty} (-1)^{n+1} \sigma^{(n)}. \quad (22)$$

As a simplified model consider only the first two graphs shown in Fig. 4, assuming $\sigma^{(n)} \ll 4\sigma^{(2)} < \sigma^{(1)}$ with $n > 2$. Then, the total cross section becomes $\sigma_{\text{tot}} = \sigma^{(1)} - \sigma^{(2)}$,

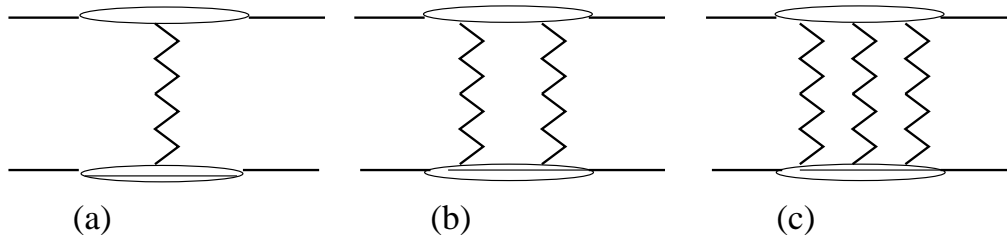


Figure 4. Hadron-hadron scattering via pomeron exchange: (a) one-Pomeron, (b) two-Pomeron, and (c) three-Pomeron exchange graphs.

where $\sigma^{(1)}$ and $\sigma^{(2)}$ are the cross sections of the one- and two-pomeron exchange graphs, respectively. The energy-dependence of the two-pomeron cross section is directly linked to that of $\sigma^{(1)} \sim s^\epsilon$ and turns out to be $\sigma^{(2)} \sim s^{2\epsilon}$. The two-pomeron cross section grows faster with energy than the one-Pomeron cross section. Since its contribution is negative, this leads to a weaker energy-dependence of the total cross section than in the single-Pomeron exchange model and a smaller effective Pomeron intercept. It also breaks Regge factorization.

Interestingly, according to the Abramovski, Gribov, Kancheli (AGK) cancellation theorem, the contribution of the two-pomeron graph to the inclusive inelastic single-particle cross section vanishes [25]. Analogously, the factorization violating contributions due to multi-Pomeron exchange graphs cancel out in all orders. This means that only the one-Pomeron graph determines the inclusive particle cross section in the central region. Consequently, a study of the energy-dependence of the single-particle inclusive spectrum should allow to measure the value of the Pomeron intercept in soft hadronic interactions, in a way which is unaffected by multi-Pomeron (or screening) effects.

The results of such an analysis is shown in figure 5 [24]. The authors use a double-Regge expansion, valid at high energies and in the central region of centre-of-mass rapidity ($y = 0$), which predicts the energy-dependence

$$\frac{d\sigma}{dy}_{y=0} = a_{PP} s^\Delta + a_{RP} s^{(2\Delta-1)/4} + a_{RR} s^{-1/2} \quad (23)$$

where the a -parameters are Reggeon couplings and $1 + \Delta$ is the value of the Pomeron intercept, unaffected by multi-Pomeron absorptive effects. The fit yields $\Delta = 0.170 \pm 0.008$, for negative particle (c^-) production and $\Delta = 0.167 \pm 0.024$ for K_S^0 inclusive production. As anticipated above, this is substantially larger than the effective intercept $\simeq 0.08$ deduced from the s -dependence of hadron-hadron total cross sections which is, however, affected by the rescattering contributions.

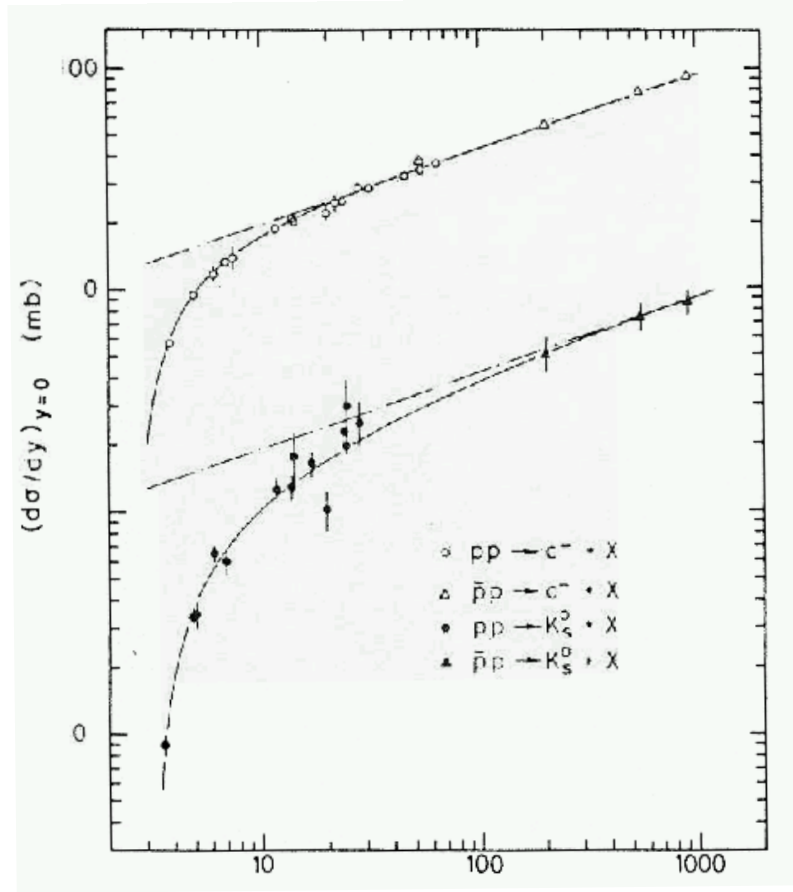


Figure 5. Cross sections of negatively charged particles and K_S^0 in the reactions $pp \rightarrow c^- + X$, $p\bar{p} \rightarrow c^- + X$, $pp \rightarrow K_S^0 + X$ and $p\bar{p} \rightarrow K_S^0 + X$ in the central centre-of-mass rapidity region, $(d\sigma/dy)_{y=0}$. c^- stands for a negatively charged hadron. The solid curves are fits with the double-Regge expression (23) with a super-critical Pomeron: $as^\Delta + bs^{(2\Delta-1)/4} + cs^{-1/2}$ yielding $\Delta \simeq 0.17$ for all reactions. The dashed lines represent the s^Δ term. For references to data see [24].

In [26] it is argued that the “bare” value of Δ is still larger, since renormalization effects induced by Pomeron-Pomeron interactions lower its effective value. The correction is estimated to be ~ 0.14 . In all, this implies that the bare Pomeron intercept could be as large as 1.3 and thus comparable (see below) to what is measured in deep-inelastic scattering. For the latter process, absorption effects due to multi-Pomeron exchange are expected to be much smaller than in soft hadronic collisions, due to the short interaction time, and to diminish with increasing Q^2 with the result that the Pomeron intercept measured in DIS could come close to that of the bare Pomeron “active” in soft hadron collisions.

Let us note also that the parameterization (23) predicts cross sections for negatively charged particles and K_S^0 of 251 ± 26 mb and 25 ± 7 mb, respectively, at the LHC.

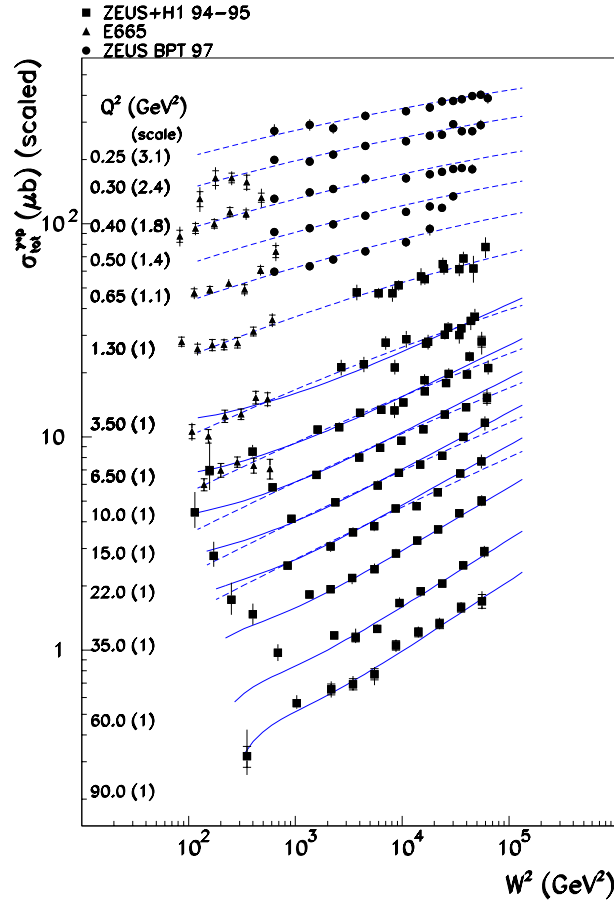


Figure 6. γ^*p cross section as a function of W^2 at various Q^2 , shown on the left side together with the scale factor applied to the data for better visibility. The full lines show a QCD-fit [27], the dashed lines are a fit by the Golec-Biernat Wüsthoff saturation model [28]. From [29].

3.2. The γ^*p total cross section at HERA

The measurement of the total γ^*p cross section as a function of Q^2 and W is one of the major achievements of the experiments at HERA. Some results are shown in Fig. 6 [31]. Remembering that $1/\sqrt{Q^2} = R_{\gamma^*}$ determines the transverse distance which the photon can resolve, we note that for small Q^2 (large R_{γ^*}) the cross section has a hadron-like increase with W : the photon acts like a hadron. With increasing Q^2 , the rise with W becomes stronger: the photon shrinks and becomes more and more point-like.

Parameterizing the W -dependence as $\sigma_{tot}^{\gamma^*p} \sim (W^2)^{\lambda_{tot}}$, one obtains the results shown in figure 7. Within the measured range, λ_{tot} increases linearly with $\log(Q^2)$ from a value $\simeq 0.08$ at low Q^2 , the same as in hadron-hadron interactions, to $\simeq 0.35$ at the highest Q^2 . These data were also analysed in [32]. If interpreted in terms of Regge exchanges, it is clear that for γ^*p collisions, “universality” of the trajectory parameters no longer holds: $\alpha_P(0)$ depends on Q^2 , and a continuous transition is seen between the soft regime and that where a “small-size” γ^* hits a proton. The dynamics evolves in a continuous

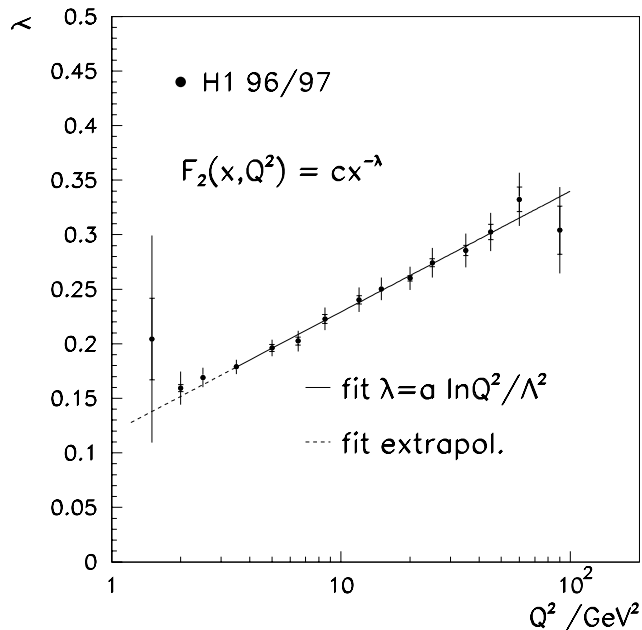


Figure 7. The exponent λ_{tot} in $\sigma_{tot}^{\gamma^*p} \sim (W^2)^{\lambda_{tot}}$, versus Q^2 . The full line shows a fit to the form indicated with $a = 0.0481 \pm 0.0013(\text{stat}) \pm 0.0037(\text{syst})$ and $\Lambda = 292 \pm 20(\text{stat}) \pm 51(\text{syst})$ MeV. Extrapolation to $Q^2 = 0.48$ GeV² gives a value of 0.08[30].

manner. Evidently, as is well-known, the results for “small-size” virtual photons can be (partly) interpreted in terms of perturbative QCD radiation and the familiar parton-density evolution equations.

3.3. Elastic scattering and forward slope

3.3.1. Hadron hadron interactions. Figure 8a shows data on the forward elastic slope in pp and $\bar{p}p$ interactions. The shrinkage of the diffractive peak with \sqrt{s} , expected from Regge theory is clearly seen. Expressed in geometrical or optical terms, the “effective interaction radius” of the proton becomes larger with increasing s , as schematically illustrated in figure 2.

The values of the slopes are in rough agreement with what is expected for (optical) diffraction on a “black” fully absorbing disk of radius R for which $B = R^2/4$. For a proton with $R \approx 1/m_\pi$ (m_π is the pion mass), B is expected to have a value of 13 GeV⁻² which compares well with the data. However, for scattering on a black disk, $\sigma_{el}/\sigma_T = 1/2$, whereas experiment, figure 8b, shows a value between 1/5 and 1/4 at high s . This means that the proton is semi-transparent, even at zero impact parameter as shown experimentally in [33]. Indeed, since the wavefunctions of the hadrons entering the collision are a superposition of states, some will be fully absorbed, while others will pass through almost unaffected. This agrees with the idea of color transparency in QCD (see section 6.3.2). Such a mixture of states with very different absorption probabilities will be essential for inelastic diffraction to occur, see section 5.2.

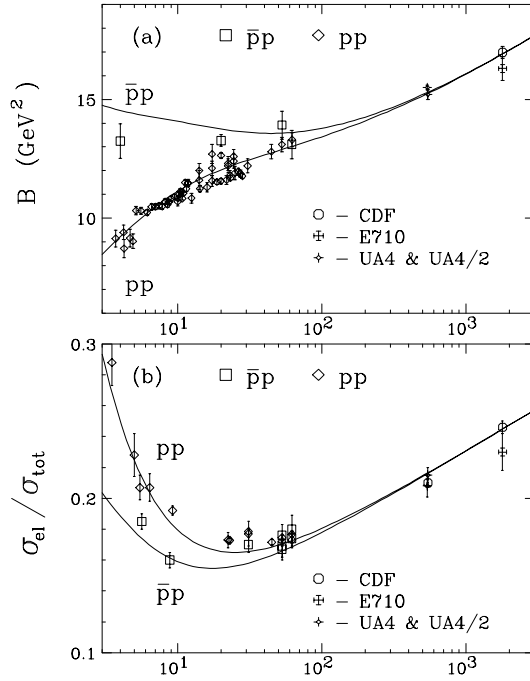


Figure 8. (a) slope parameter $B(s)$, (b) ratio of elastic to total cross section versus \sqrt{s} for $\bar{p}p/pp$ interactions. The solid lines are Regge fits. For details see [21].

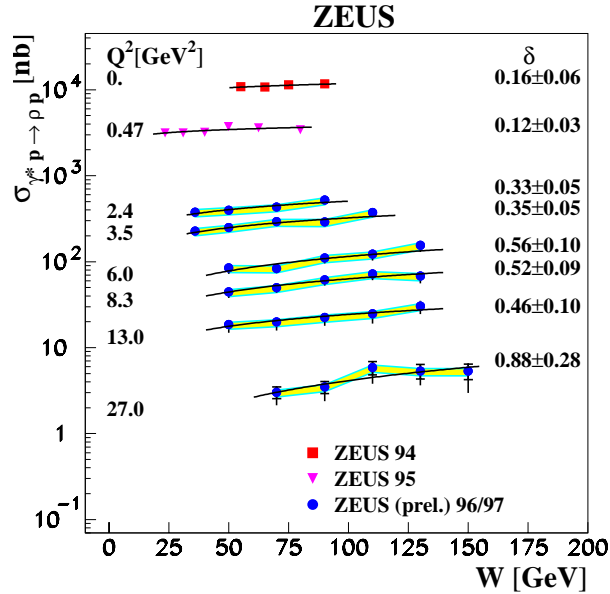


Figure 9. W dependence of the cross section $\sigma(\gamma^* p \rightarrow \rho^0 p)$ for various Q^2 values. The data for $Q^2 < 1 \text{ GeV}^2$ obtained previously [34] are also shown. The solid lines show a fit with $\sigma_{\gamma^* p \rightarrow \rho^0 p} \sim W^\delta$. The shaded area indicates normalization uncertainties due to proton dissociation background. From [35].

3.3.2. Real and virtual photon quasi-elastic scattering. Among the many results now available (for a review see [36]), figure 9 shows, as an example, DIS measurements of

the W -dependence of elastic ρ^0 electroproduction as a function of Q^2 . For each Q^2 interval, the cross section is assumed to be of the form W^δ . In the same manner as for the γ^*p total cross section, the data suggest a marked increase of δ when Q^2 enters a regime where pQCD becomes relevant. However, the errors remain sizable and, in W -regions where the DIS data overlap ($3.5 \leq Q^2 \leq 13.0$ GeV²), the Q^2 -dependence of δ is statistically not yet very significant. Measurements at larger Q^2 are needed to clarify this important issue.

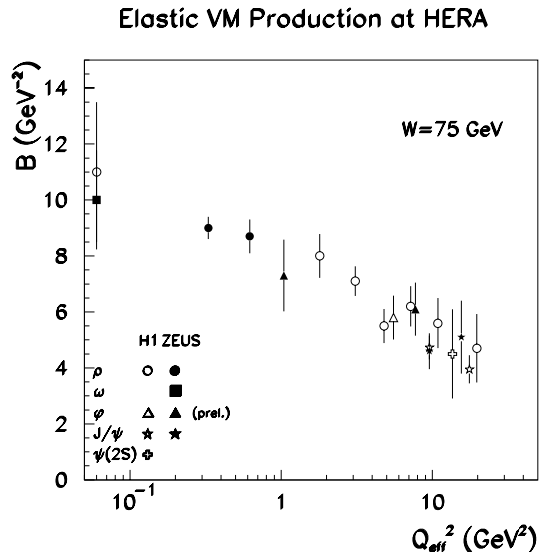


Figure 10. Slope parameter $B(s)$ as a function of Q_{eff}^2 ; $Q_{eff}^2 = Q^2$ for ρ and ω , $Q_{eff}^2 = Q^2 + M_\phi^2$ for ϕ , $Q_{eff}^2 = Q^2 + M_{J/\psi}^2$ for J/ψ . From [29].

As to the shape of the diffractive peak, figure 10 shows a compilation [29] of the slope B , at fixed W , as a function of an effective scale, $Q_{eff}^2 = Q^2 + m_V^2$, for various vector mesons with mass m_V . The slope becomes smaller with increasing Q_{eff}^2 . In the photoproduction region, $Q_{eff}^2 = 0$, the slopes for ρ and ω are quite similar to those observed in proton-proton scattering, see figure 8. At higher Q_{eff}^2 , they are considerably smaller, approximately half of that observed in proton-proton scattering. The effective interaction region reduces to about that of a single proton, as expected for a projectile which becomes more point-like as Q^2 grows. At the same time the total cross section itself grows faster with W than in hadron interactions.

For elastic J/ψ photoproduction, ZEUS recently measured (see [37]) the differential cross-section, $d\sigma/dt \propto (W)^{2\alpha_P(t)-2}$, in the energy-range $20 < W < 290$ GeV, and $|t| < 1.25$ GeV². From the t -slope in bins of W , yielding e.g. $B = 4.3 \pm 0.08$ (stat) $_{-0.41}^{+0.16}$ (syst) GeV⁻² at $W = 90$ GeV, one derives $\alpha_P(0) = 1.201 \pm 0.013$ (stat) $_{-0.011}^{+0.003}$ (syst) and $\alpha'_P = 0.126 \pm 0.029$ (stat) $_{-0.028}^{+0.015}$ (syst) GeV⁻². The latter value implies that shrinkage is smaller than in soft hadronic collision but not negligible. This was predicted in [38].

A recent first-time ZEUS measurement [35] of the leading trajectory parameters from exclusive ρ production in DIS, $\gamma^*p \rightarrow \rho^0p$, ($1 < Q^2 < 40 \text{ GeV}^2$), yielded $\alpha_P(0) = 1.14 \pm 0.01 \text{ (stat)}_{-0.03}^{+0.03} \text{ (syst)}$, $\alpha'_P = 0.04 \pm 0.07 \text{ (stat)}_{-0.04}^{+0.13} \text{ (syst)} \text{ GeV}^{-2}$. While not conclusive, given the errors, this measurement also suggests a smaller value of α'_P than that of the “soft” Pomeron ($\alpha'_P \approx 0.25 \text{ GeV}^{-2}$).

From a measurement of the spin-density matrix of the ρ^0 decay, ZEUS [35] also extracted σ_L/σ_T , the ratio of the cross section for longitudinally and transversely polarized γ^* , as a function of Q^2 and W . The ratio strongly increases with Q^2 but is found to be independent of W , a somewhat surprising result given the expectation that at large Q^2 the average transverse size of the longitudinally polarized γ^* is much smaller than that of a transversely polarized γ^* [39].

3.3.3. Brief summary. Although more precise measurements are evidently needed, and forthcoming, the present data on total and elastic differential cross sections suggest a clear trend. As for real hadrons, for near-on-shell photons fluctuating into light vector mesons, (ρ , ϕ) and which have large (order 1 fm) transverse extensions, inversely proportional to the Compton wavelength of the light quarks in the meson, the effective Pomeron trajectory $\alpha_P(t)$ is close to that of soft collisions. For heavier vector mesons (e.g. J/ψ), which are characterized by a smaller transverse size, or in DIS, present data provide some indication for a weaker shrinkage, with α'_P smaller than the “soft” value 0.25 GeV^{-2} . At the same time, the effective intercept $\alpha_P(0)$ grows with decreasing size R_{γ^*} . The transition from the soft hadron-like regime to DIS is a smooth one.

4. Inelastic diffraction

4.1. Experimental signatures

In contrast to forward elastic scattering, which beautifully reflects the wave-nature of the particles, the phenomenon of diffraction dissociation, predicted by Good and Walker [40], has no classical analogue. For hadron-hadron scattering, it corresponds to quasi-elastic scattering between the two hadrons, where, in single diffraction, one of them is excited into a higher mass state retaining its quantum numbers. This *coherent* excitation, illustrated in figure 11 for single-diffraction, requires not only small transverse (ΔP_T) but also small longitudinal (ΔP_L) momentum transfer. This leads to the *coherence condition* (see e.g. [41, 42]):

$$\xi \approx \frac{M_X^2}{s} < \frac{m_\pi}{m_p} \approx 0.1 - 0.2. \quad (24)$$

The coherence condition arises from the need to conserve the coherence of the quasi-elastically scattered target and implies that the diffractive mass M_X cannot be too large. For zero-angle production the minimum four-momentum transfer at which the mass M_X can be produced is $|t_{min}| = [(M_X^2 - m_p^2)/2p]^2$, with p the incident momentum in the target rest frame. In the transition, the wavenumber k of the incident hadron varies

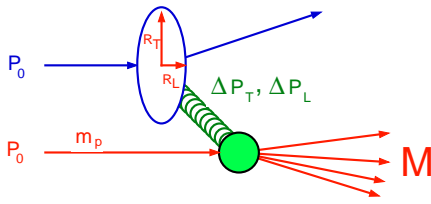


Figure 11. Single diffractive dissociation. The invariant mass of the produced hadrons, M , is denoted by M_X in the main text. From [43].

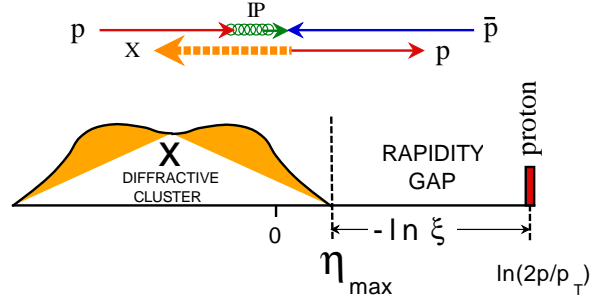


Figure 12. Topology for $p\bar{p} \rightarrow pX$ [43].

by an amount $\Delta k \propto \sqrt{|t_{min}|}$. The condition of coherence follows from the requirement that the wavenumber changes little during the passage through the target, so that the waves describing the target before and after the interaction can stay in phase. For DIS kinematics, the minimum value of t required to produce a given M_X from a target with mass m_T is $|t_{min}| \simeq m_T^2(M_X^2 + Q^2)^2/W^4$. For a typical hadronic radius of 1 fm, $M_X^2 < 0.2 W^2$.

The generic topology of a single-diffractive (here $\bar{p}p$) event is illustrated in figure 12. The upper-limit on M_X implies that the diffractive hadronic final states exhibit a large rapidity gap between the quasi-elastically scattered proton and the dissociation products X of the \bar{p} . The width of the gap in (pseudo-)rapidity space measured from the rapidity of the initial-state proton is $\Delta\eta \approx \ln \frac{1}{\xi}$. In collider experiments diffractive events are thus identified either by detecting directly a “fast” (“leading”) proton in a spectrometer, by the presence in the main detector of a large rapidity region devoid of hadrons (a rapidity gap), or by exploiting the characteristic $1/M_X^2$ dependence of diffraction.

Naively, the interaction is often viewed as proceeding via the emission from the proton of a Pomeron, a colorless object with vacuum quantum numbers which subsequently interacts with the \bar{p} . In QCD such an object, if it were to exist as a physical entity, must be a colour-singlet composed of quarks, antiquarks and gluons. It will become clear later, however, that such a picture is an unnecessary and probably misleading simplification of mechanism behind diffractive physics.

4.2. Hadron hadron inelastic diffraction

Evidence for an important diffractive component in the inclusive reaction $p + p \rightarrow p + X$, with excitation of large masses, was first established at the ISR by the CHLM collaboration [45]. Figure 13 shows single diffractive pp cross sections from low to high s . The diffractive enhancement becomes less and less prominent as s decreases, in line with the previous discussion about the need to maintain coherence of the target. The M_X -spectrum drops rapidly in the resonance region. Beyond that it levels-off and shows

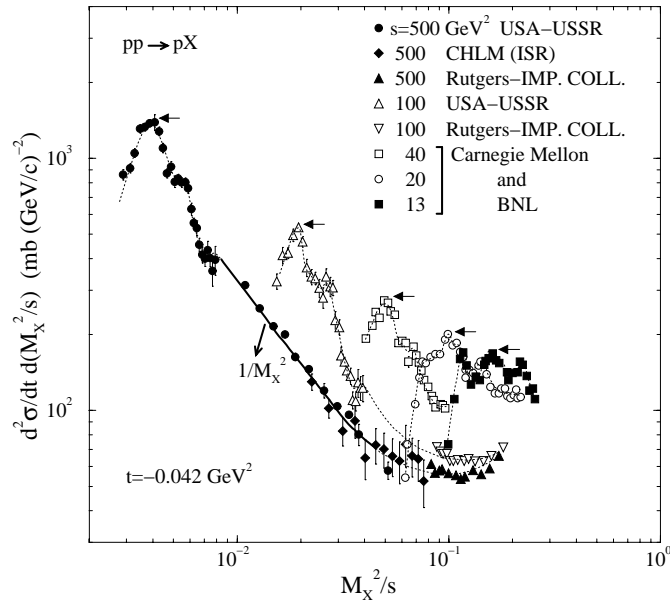


Figure 13. Single diffractive pp cross sections [42]). The figure shows how the characteristic $1/M_X^2$ (Regge) behavior of diffraction becomes manifest as s increases. The arrows indicate the low mass ($M_X \approx 2$ GeV) resonance region. From [44].

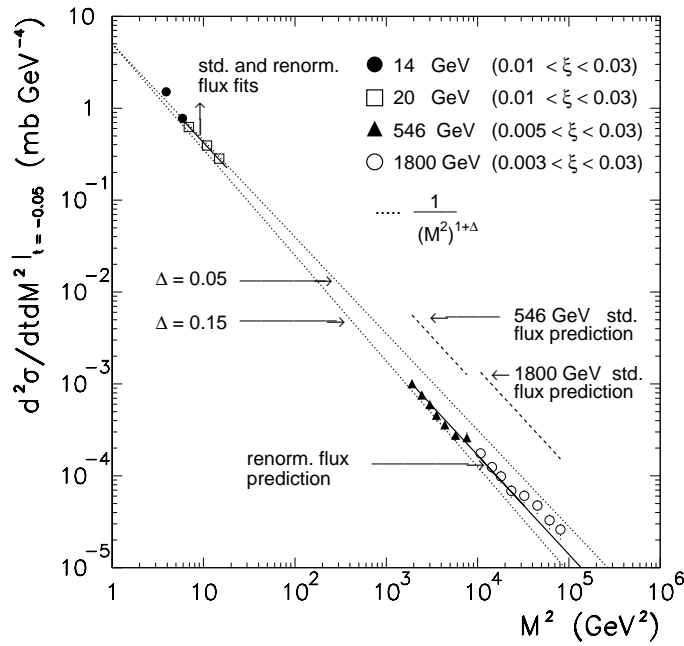


Figure 14. Cross sections $d^2\sigma_{sd}/dM_X^2 dt$ for $p + p(\bar{p}) \rightarrow p(\bar{p}) + X$ at $t = -0.05$ GeV² and $\sqrt{s} = 14, 20, 546$ and 1800 GeV. For a description of the curves see [13].

an approximate $1/M_X^2$ dependence.

A compilation of measurements [13], now plotted against M_X^2 , is shown in figure 14 for pp and $\bar{p}p$ single diffractive cross sections at $t = -0.05 \text{ GeV}^2$ (for earlier compilations see [46]). The distribution falls as $1/(M_X^2)^{1+\Delta}$ over the entire M_X region. Quite remarkably, it is independent of s over five orders of magnitude. The data are consistent with the same value of $\alpha_P(0) - 1 = \epsilon = 0.104$ (denoted Δ in the figure) as that extracted from the fit in [21] to total and elastic cross sections data.

The $1/M_X^2$ scaling shown by the data in figure 14 implies that, since ϵ is small, the rapidity-gap distribution, $d^2\sigma_{sd}/dt d\Delta\eta$ is nearly independent of s . In Regge models of diffraction, this distribution is related to the ‘‘Pomeron flux’’, see equation (18). Such a weak energy-dependence must reflect a fundamental, but not yet understood, property of the baryon ‘‘re-formation’’ process in the final state. A strict energy-independence would be consistent with *short-range order*[47], a basic property of multiparticle production.

4.3. Inclusive diffraction at HERA

In DIS at small x measured at HERA, inelastic diffraction occurs at a rate of $\mathcal{O}(10\%)$ of all events [48]. Although it surprised many in the pQCD community, it had been anticipated even before the advent of QCD [49]. It was also predicted from Regge theory [50]. The occurrence of such diffractive events, also called ‘‘Large Rapidity Gap events’’ are indeed difficult to understand in the parton picture on the basis of pQCD alone.

The experimental effort at HERA has concentrated on measurements of the diffractive part, $F_2^{D(3)}$, of the structure function F_2 , equation (7). The data have been reviewed on many occasions and details can be found in [1, 2, 51, 52].

New preliminary H1 1997 inclusive diffractive data [15] have been used to extract $\alpha_P(0)$ from the ξ -dependence of $F_2^{D(3)}(\beta, Q^2, x_P)$ with much increased precision, yielding $\alpha_P(0) = 1.173 \pm 0.018(\text{stat.}) \pm 0.017(\text{syst.})_{-0.035}^{+0.063}(\text{model})$. This value is not much higher than $\alpha_P(0) \simeq 1.1$ in soft processes. As figure 15 shows, there is no evidence for a systematic variation with Q^2 . The data further suggest that the effective intercept for $\sigma_T(\gamma^*p)$ is larger than that of the diffractive contribution at high Q^2 .

Another striking HERA result, first obtained by ZEUS [14], is illustrated in figure 16 and in figure 17 which shows more recent H1 measurements [15]. For Q^2 and M_X (and thus β) fixed, the relative rate of diffractive events is nearly W -independent, except at very small β . Standard triple-Regge theory, without multi-Pomeron exchange, predicts an increase as $(W^2)^\epsilon$, in clear disagreement with data.

As discussed in [54], no adequate explanation within purely pQCD of the constancy of the mentioned ratio is known at present. The authors conclude that the non-perturbative QCD contribution to diffractive production is essential. Indeed, constancy of the ratio is obtained quite naturally in the quasi-classical gluon field approach (see Buchmüller in [2]). It is also correctly predicted in the GBW-model [28]. There it is a consequence of the basic assumption that the cross section of the system radiated off

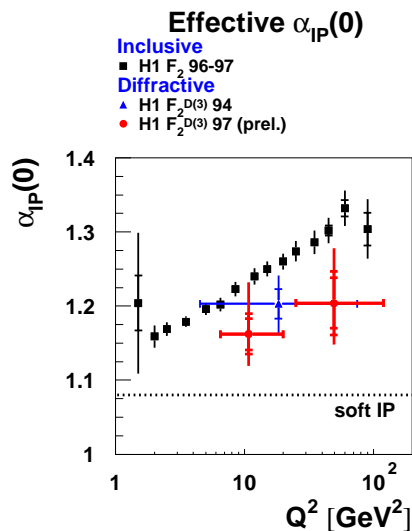


Figure 15. H1: effective value of $\alpha_P(0)$ as function of Q^2 : \bullet extracted from $F_2^{D(3)}$; \blacksquare from a fit of $F_2(x, Q^2)$ to the form $x^{-\lambda(Q^2)}$; \blacktriangle H1 1994 data [53]. From [15].

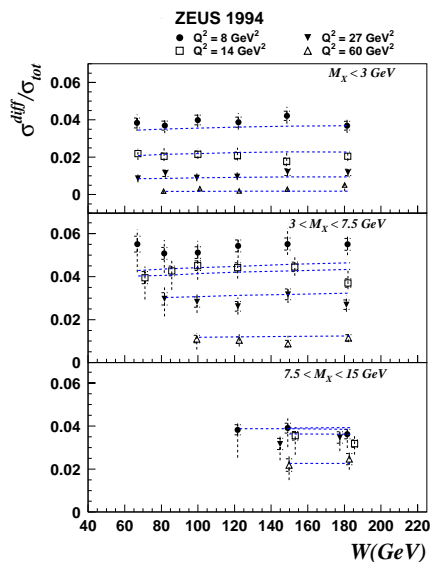


Figure 16. Ratio of diffractive and total cross sections at fixed values of Q^2 , for different regions of the invariant diffractive mass M_X . The lines are predictions of the saturation model [28].

the γ^* partonic fluctuations saturates once this system has acquired a large transverse extension and is thus non-perturbative.

4.3.1. An interlude: Leading baryons, the energy-loss spectrum. Inclusive diffraction shows a fractional proton energy-loss spectrum of the form given in equation (20). For $\epsilon = 0$ this intriguingly resembles a soft bremsstrahlung spectrum. Early QCD-models

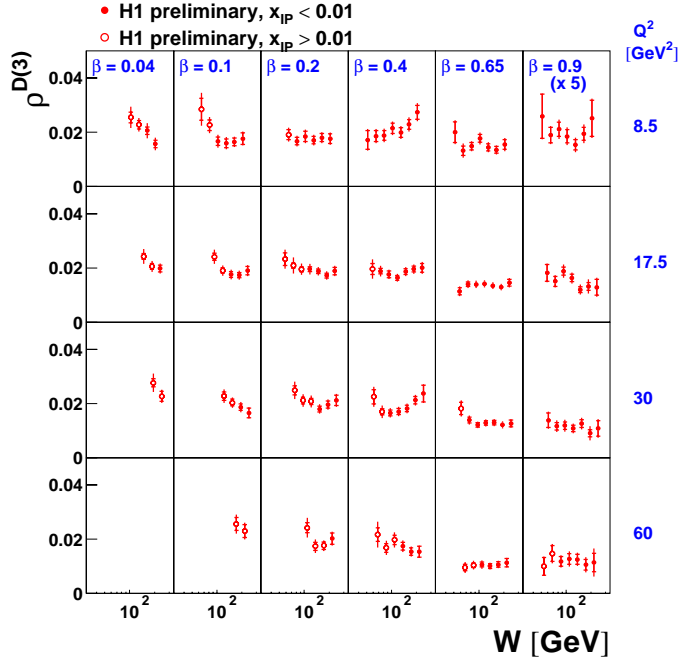


Figure 17. Recent H1 measurements of $\rho^{D(3)}$, the ratio of the diffractive to the inclusive cross section versus W . Data at $\beta = 0.9$ are scaled by a factor of five [15].

for diffraction have been proposed based on this analogy which indeed predict a $1/M_X^2$ spectrum [57]. In this context it is interesting to recall a calculation of the leading-particle (LP) energy loss using a QED soft radiation analogy by Stodolsky [58].

Assume that a “leading” particle loses energy analogously to an electron which emits soft photons via bremsstrahlung. If ζ is the total energy lost by the incident hadron which has initial energy E_0 , the probability to radiate N particles of total energy ζ , with N_i of them having energy ω_i , is given by

$$P_N(\zeta) = \sum_{N_1, N_2, \dots} P(N_1) P(N_2) \cdots \delta(\zeta - N_1\omega_1 - N_2\omega_2 - \cdots) \times \delta(N - N_1 - N_2 - \cdots), \quad (25)$$

where

$$P(N_i) = \frac{[(d\bar{N}/d\omega)d\omega]^{N_i}}{N_i!} \exp\left(-\frac{d\bar{N}}{d\omega}d\omega\right), \quad (26)$$

is the Poisson probability (valid in QED for soft radiation) for N_i emissions in the energy-interval $\omega_i, \omega_i + d\omega$, with $[(d\bar{N}/d\omega)d\omega]$ their mean number. Setting $d\bar{N}/d\omega = \lambda/\omega$ and summing over all N one finds after a lengthy calculation the surprisingly simple result

$$f(z) \equiv \frac{1}{\sigma} \frac{d\sigma}{dz} = \lambda (1 - |z|)^{\lambda-1}; \quad (27)$$

with z the fractional energy E/E_0 of the proton. For $\lambda \simeq 1$ one obtains a *flat distribution*.

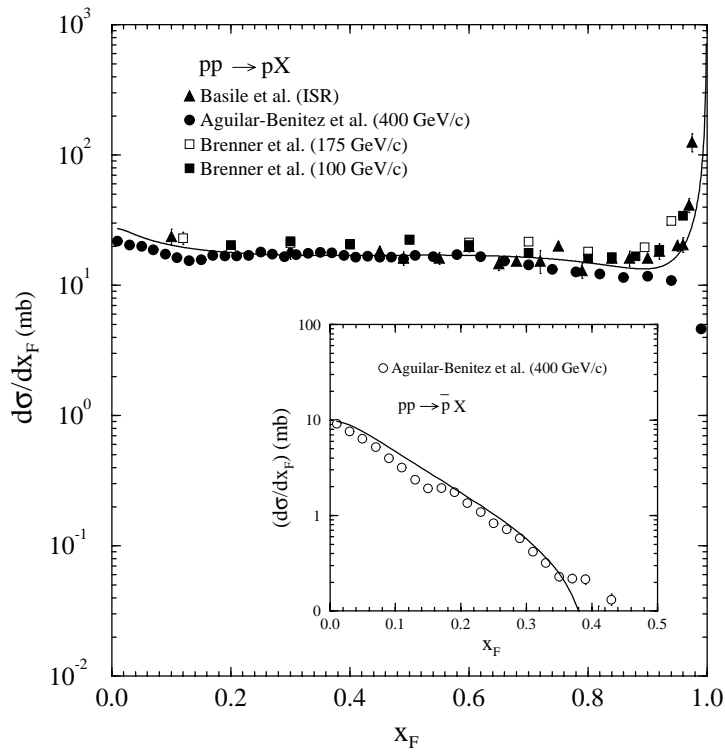


Figure 18. Inclusive spectrum for the reactions $pp \rightarrow pX$ and $pp \rightarrow \bar{p}X$ (insert). From [55].

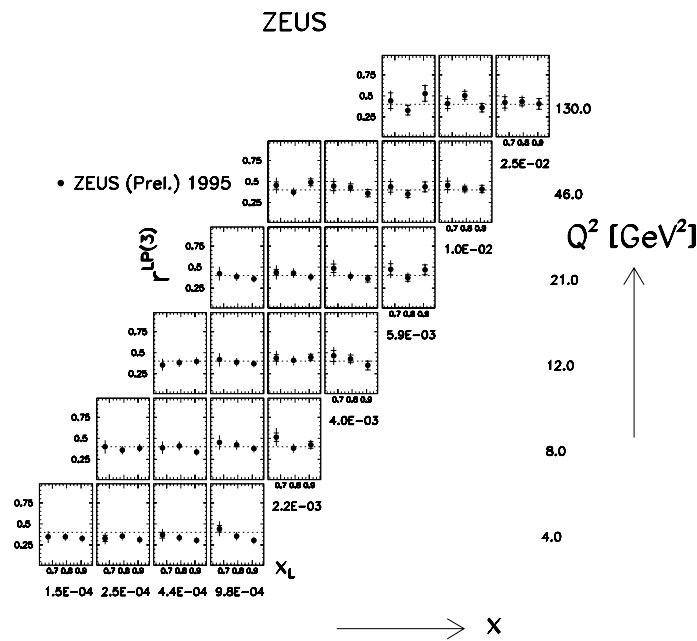


Figure 19. The fraction of leading protons, measured with the ZEUS Leading Proton Spectrometer, as a function of $x_L = 1 - \xi$ in bins of x and Q^2 . From [56].

The previous calculation assumed Poisson emission which disagrees with experimental observations (and pQCD predictions). Generalizing to an emission process where the multiplicity distribution obeys Koba-Nielsen-Olesen (KNO) scaling (valid in pQCD [59, 60]), $\langle N \rangle P(N) = \Psi(N/\langle N \rangle)$ with $\Psi(u)$ energy-independent, one finds [61]

$$\frac{1}{\sigma} \frac{d\sigma}{dz} = \int_0^\infty d(\lambda/\bar{\lambda}) \Psi(\lambda/\bar{\lambda}) \lambda(1-z)^{1-\lambda}. \quad (28)$$

The mean number of radiated objects is $\langle N \rangle = \bar{\lambda} \ln(s/s_0)$ with s_0 a scale parameter. A flat z spectrum is recovered for $\bar{\lambda} \simeq 1$. The parameter $\bar{\lambda}$ is the mean number of emitted objects per unit of rapidity. For comparison with experimental data one has to assume that these objects (they were called “clusters” in ancient times) are resonances or higher-mass states decaying on average into two or three final-state particles. A density $\bar{\lambda} \approx 1$ is therefore a reasonable number.

In the limit $z \rightarrow 1$, and for $\Psi(u) \sim u^\beta$ near $u = 0$, one obtains

$$\frac{1}{\sigma} \frac{d\sigma}{dz} \sim \Gamma(\beta + 2) \frac{1}{1-z} \frac{1}{[\ln(1-z)^{-1}]^{\beta+2}}. \quad (29)$$

Thus, besides being flat away from $z = 1$, the spectrum develops a diffractive-like peak at large z . Ignoring the logarithmic factor, this result coincides with equation (20) for $\alpha_P(0) = 1$. In fact, in triple-Regge language, the full expression, equation (29), corresponds to a *Pomeron cut*, and not a simple *Pomeron pole*, in line with general theoretical expectation. In this model, the enhancement near $z = 1$ is due to low-multiplicity events. The detailed shape of the spectrum is, therefore, determined by that of the KNO function at small values of u .

We find it remarkable that the quite simple and reasonable assumptions leading to equation (28) are sufficient to capture essential aspects of the LP spectrum and its ‘diffractive limit’, $z \rightarrow 1$. If both $\bar{\lambda}$ and Ψ vary slowly with energy, the same will hold for the LP spectrum and for the diffractive peak and is not in disagreement with experiment.

The “flatness” of the leading proton spectrum is well-known from hadron-hadron collisions. An example for pp interactions is shown in figure 18. The same flatness is seen in DIS data (an example from ZEUS is shown in figure 19). Although the spectra are found to be independent of x and Q^2 in the DIS regime, a small but significant increase of the rate with Q^2 is now seen in the low- Q^2 region [56].

Whereas diffractive data at very small ξ and so-called Leading-Baryon data at larger ξ , outside of the diffractive region, are usually analyzed separately, our previous discussion argues in favour of combined analyses of such data. This has recently been done by the authors of [44] who combined diffractive structure function measurements with Leading-Proton and Leading-Neutron results from H1. Results are shown in figure 20 [44] which displays ξF_2^{LP} and ξF_2^D as functions of ξ . A combined triple-Regge fit, including Pomeron, Reggeon and pion exchange contributions yields $\alpha_P(0) = 1.250 \pm 0.023$ and a Reggeon trajectory compatible with f_2 exchange: $\alpha_{\mathbb{R}}(0) = 0.770 \pm 0.030$. Note the somewhat larger value of $\alpha_P(0)$ than the recent H1 measurement quoted in section 4.3.

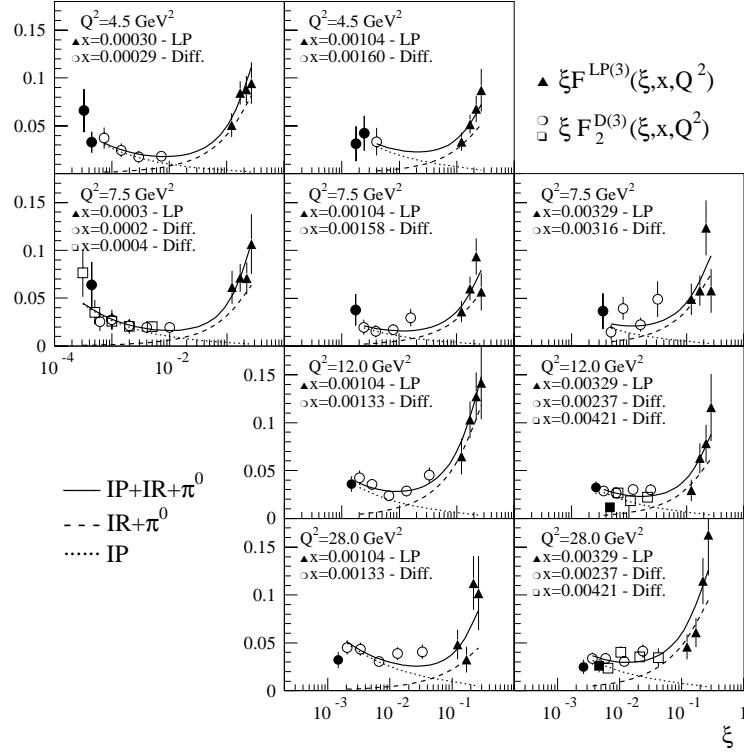


Figure 20. Diffractive (Diff, open circles and open squares) and leading proton (LP, black triangles) structure function data vs. ξ , for fixed x and Q^2 . The figure combines, in each plot, the diffractive and leading proton H1 data with similar values of x and Q^2 . The quoted Q^2 values are those of the diffractive data; the corresponding Leading Proton values are $Q^2 = 4.4, 7.5, 13.3$ and 28.6 GeV^2 . The black circles and black squares are data with $M_X < 2$ GeV . The plotted curves represent a global fit: total (solid line), pomeron (dotted line) and reggeon plus pion contributions (dashed line). For details and references see [44].

5. Unitarity

The importance of unitarity is not always sufficiently appreciated. This section is therefore devoted to a description of its main aspects and implications.

The unitarity of the scattering matrix, T , implies close relationships between total cross sections, the elastic scattering amplitude and the amplitudes of inelastic final states. The unitarity relation between states $|i\rangle$ and $|f\rangle$ reads

$$2\text{Im} \langle f|T|i\rangle = \sum_{|e\rangle\langle e|} \langle f|T^+|e\rangle\langle e|T|i\rangle + \sum_{|n\rangle\langle n|} \langle f|T^+|n\rangle\langle n|T|i\rangle, \quad (30)$$

where $\sum_{|e\rangle\langle e|}$ stands for summation and integration over all possible *elastic* intermediate states $|e\rangle$. The second term is the contribution from all possible inelastic states; $|i\rangle$ is the initial and $|f\rangle$ an *arbitrary* final state.

For forward elastic scattering, $t = 0$ ($|i\rangle \equiv |f\rangle$) equation (30) immediately leads to the optical theorem. However, the relation has much wider consequences since the state

$|f\rangle$ can be any state. It shows that the imaginary part of the amplitude of any particular final state $\langle f|T|i\rangle$ in general receives contributions from all other final states. Such “unitarization effects” will be small only if the “overlap” ($\langle f|T|n\rangle\langle n|T|i\rangle$) of the states $|i\rangle, |f\rangle$ with the states $|n\rangle$ happens to be small. This will, therefore, depend crucially on the topology in momentum space of the inelastic states and on the phases of the amplitudes.

The two terms on the right-hand side of equation (30) are called the elastic and inelastic overlap functions, respectively, and were first introduced by Van Hove [62]. For elastic scattering (and neglecting the real part), we see that the amplitude can, in principle, be calculated from the knowledge of the inelastic final states. This is the so-called s -channel approach to diffractive scattering. It provides an alternative to the t -channel approach in which the diffractive amplitudes are analyzed in terms of their singularities, poles and cuts, in the complex angular momentum plane.

An important result is obtained (valid only at high s) when equation (30) is written in impact-parameter (\vec{b}) space^{||}. Using angular momentum conservation one finds

$$2\text{Im } \mathcal{A}_{el}(s, b) = |\mathcal{A}_{el}(s, b)|^2 + G_{in}(s, b). \quad (31)$$

Here $\mathcal{A}_{el}(s, b)$ is the elastic amplitude; $G_{in}(s, b)$, the inelastic overlap function, is the contribution from all inelastic channels. From equation (31) follows that $\text{Im } \mathcal{A}_{el}(s, b)$ at impact parameter b is generated by the absorption into the inelastic channels *at the same* impact parameter: “unitarity is diagonal in b -space”.

For $\text{Re } \mathcal{A}_{el} = 0$, equation (31) can be solved easily for \mathcal{A}_{el} if $G_{in}(s, b)$ is known. Alternatively, knowledge of $\mathcal{A}_{el}(s, b, t)$ can be used to determine $G_{in}(s, b)$ (see e.g. [33]). For DIS, it is presently unknown but of great interest.

Equation (31) has the general solution

$$G_{in}(s, b) = 1 - e^{-\Omega(s, b)} \quad (32)$$

$$\mathcal{A}_{el}(s, b) = i \cdot \left\{ 1 - e^{-\frac{\Omega(s, b)}{2} + i\chi(s, b)} \right\}. \quad (33)$$

The “opacity” function or eikonal, $\Omega(b)$, and the phase $\chi(s, b)$ are arbitrary real functions. The former has a simple meaning: $\exp[-\Omega(b)]$ is the probability that *no inelastic* interactions with the target occur. We further have the general relations

$$\sigma_{el}(s) = \int d^2b |\mathcal{A}_{el}(s, b)|^2, \quad (34)$$

$$\sigma_T(s) = 2 \int d^2b \text{Im } \mathcal{A}_{el}(s, b), \quad (35)$$

$$\sigma_{in}(s) = \int d^2b [2\text{Im } \mathcal{A}_{el}(s, b) - |\mathcal{A}_{el}|^2(s, b)]. \quad (36)$$

5.1. Elastic diffraction and shrinkage

For scattering on a proton, absorption into inelastic channels will be most important for values of b smaller than the proton radius. From equation (31) follows that this

^{||} For a recent mathematical discussion of the validity of this transformation at finite energies, and further references, see [63].

will generate a large imaginary elastic amplitude at the same impact parameter. The impact parameter profile will be maximum at $b = 0$, where absorption is strongest, and the elastic differential cross section, $d\sigma_{el}/dt$, sharply peaked at $t = 0$, its width reflecting transverse extension of the effective interaction region. The experimental fact that $\text{Re } \mathcal{A}_{el}$ is small at high s implies that elastic scattering can indeed be considered as the “shadow” of the inelastic channels.

The physical meaning of the slope $B(s)$ can also be understood from the shape of $G_{in}(s, b)$ and equation (30). Indeed, $G_{in}(s, b)$ is a measure of the overlap of the amplitude of a given final state with *the same* state but rotated along the incident direction over an angle θ , the elastic scattering angle. For most of the final states $|n\rangle$, the transverse momentum of produced particles, p_T , relative to the incident direction is sharply cut off, and its average increases slowly with s : the distribution in rapidity- p_T space resembles that of a uniformly filled cylinder, sometimes called a “Wilson-Feynman liquid”, with short-range correlations only between the hadrons. For such a configuration, it is easily verified that the inelastic overlap function, and thus $\text{Im } \mathcal{A}_{el}$, will fall-off as an exponential in t , at small $|t|$, with a slope determined by the mean number of particles produced and by their $\langle p_T^2 \rangle$. For example, in a model where particles are produced independently, one finds [62] (see also [64])

$$B(s) \geq \text{constant} + \langle n \rangle / \langle p_T^2 \rangle. \quad (37)$$

Consequently, $B(s)$ grows with energy like $\langle n \rangle$, the mean multiplicity of produced hadrons if $\langle p_T^2 \rangle$ is constant. This explains the shrinkage of $d\sigma_{el}/dt$. For this estimate phases of the multiparticle amplitudes are neglected. The phase of the amplitude is related to the position in space-time where the particle is produced [65], and is unknown.

Writing $\langle n \rangle = \omega_0 \Delta y = \omega_0 \ln(s/s_0)$, we see that $B(s)$ depends on the particle density in rapidity space in inelastic collisions and by the variance of the transverse momentum distributions. In more rigorous calculations, the second-order transverse momentum transfer correlation function \mathcal{C} enters in equation (37) instead of $\langle p_T^2 \rangle$ [47, 66].

This result is generic and valid in a wide class of models (see e.g. [67]). In processes where $\langle p_T^2 \rangle$ is larger than a soft scale, or large compared to $|t|$, the second term on the right-hand side of equation (37) will be unimportant and shrinkage will either be small or absent. This most likely happens in (quasi-)elastic processes where a large scale can be identified (“hard diffraction”).

Whereas the overlap of the amplitude of two “Feynman-Wilson liquids” will be negligible at large t , one realizes easily that hard jet emission will contribute to non-zero values of the overlap function at large t . This is the basic reason for the importance of very large t scattering and its connection with perturbative QCD.

In a general collision process, and γ^*p in particular, both ω_0 and $\langle p_T^2 \rangle$ can be expected to be process- and (perhaps) energy-dependent. There is no sound reason to

\mathcal{C} In pQCD “ladder-language”, this is the correlation between neighbouring propagator transverse momenta.

believe that these quantities, and thus the intercept and slope of the dominant Regge trajectory, are universal.

The arguments given show clearly the connection between properties of the final states and Regge trajectory parameters for diffractive scattering. Since the relevant dynamical quantities, here ω_0 and $\langle p_T^2 \rangle$, are clearly identified, generalization beyond the Regge framework is, at least conceptually, simple to understand.

5.2. Inelastic diffraction as a regeneration process

The possibility of inelastic diffraction has been predicted in the seminal papers by Feinberg and by Good and Walker [40]. Consider a projectile (hadron, real or virtual photon, etc.) hitting a target at rest. The projectile, being composite, can be described as a quantum-mechanical superposition of states containing various numbers, types and configurations of constituents. The various states in this superposition are likely to be absorbed in different amounts by the target. As a result, the superposition of states after the scattering is not simply proportional to the incident one. Hence, the process will, besides elastic scattering, also lead to production of inelastic states with the same internal quantum numbers as the projectile. This is the fundamental basis for inelastic diffraction and requires little more than the superposition principle of quantum mechanics, unitarity and the coherence condition, equation (24).

Assume that the projectile, $|B\rangle$, at a fixed impact parameter (\vec{b}) from the target is a linear combination of states which are eigenstates of diffraction

$$|B\rangle = \sum_k C_k |\Psi_k\rangle, \quad (38)$$

$$\text{Im}T |\Psi_k\rangle = t_k |\Psi_k\rangle, \quad (39)$$

where $\text{Im}T$ is the imaginary part of the scattering operator and the (real) eigenvalue t_k is the probability for the state $|\Psi_k\rangle$ to interact with the target. The eigenvalues or absorption coefficients t_k of course vary with \vec{b} . The states are normalized so that $\langle B|B\rangle = \sum_k |C_k|^2 = 1$. From equation (38) and equation (39) one easily derives

$$d\sigma_T/d^2b = 2 \langle t \rangle, \quad (40)$$

$$d\sigma_{\text{el}}/d^2b = \langle t \rangle^2. \quad (41)$$

The cross section for inelastic diffractive production, with elastic scattering removed, is

$$d\sigma_{\text{diff}}^{\text{inel}}/d^2b = \langle t^2 \rangle - \langle t \rangle^2. \quad (42)$$

The brackets $\langle \dots \rangle$ denote an average of t_k or t_k^2 , weighted according to their probability of occurrence, $|C_k|^2$, in $|B\rangle$. We note the important result that inelastic diffraction is proportional to the variance in cross sections of the diagonal channels. Elastic scattering, on the other hand, is proportional to their mean value. Equations (40)-(42) further imply the upper (Pumplin) bound [68]

$$\sigma_{\text{diff}}(b) + \sigma_{\text{el}}(b) \leq \frac{1}{2} \sigma_{\text{tot}}(b). \quad (43)$$

From equation (42) follows that, if the variance is zero (e.g. when all states are absorbed with the same strength) there is no inelastic diffraction. Diffraction will be strongest in regions of b -space where absorption shows the strongest variation i.e. at the “edges” of the target: hadronic inelastic diffraction is more peripheral than the elastic process which is largest at small b . Further, in the case of complete absorption at a given b , inelastic diffraction vanishes at the same b .

Note that for virtual photon scattering, the purely elastic reaction can be neglected. In this case, the term $\langle t \rangle^2$ in equation (42) is absent. For real and virtual photon-hadron interactions, very little is known experimentally about the impact parameter profile. It requires a measurement of the t -dependence over a wide range in t . For elastic ρ production it was studied for the first time in [69], following the method of Amaldi and Schubert [33].

As remarked in [70], “The increase of σ_T (in DIS) with energy occurs because some regions of impact parameter are changing from grey to black and regions at larger b are going from white (no absorption) to grey. However, the region where absorption shows the strongest variation, and which contributes to diffraction, grows less rapidly than those b -regions giving elastic and highly inelastic scattering. This would explain the observation that the inclusive diffractive cross section grows less rapidly than expected from Regge arguments (cfr. figure 17). Regge theory is indeed expected to hold for those regions in b where the absorption is weak. Regions of large absorption then correspond to multiple Pomeron exchanges.”

6. A generic picture of high energy collisions

Well before the advent of QCD, and inspired by the ideas of Ioffe, Feinberg, Gribov, Pomeranchuk and others, a basic, although semi-quantitative, understanding of the space-time evolution of a high-energy scattering process was developed [49, 71, 72]. It testifies to the profoundness of these ideas that, in spite of major developments in the field of strong interactions, the physical picture then developed still remains valid to a very large extent. Perturbative QCD has allowed us to clarify many issues, and produce crisp quantitative predictions in some cases, but the ideas then formulated, reaching well beyond pQCD, continue to be of great value. They provide a view of the collision dynamics which is simple enough to help develop intuition, provide physical insight and, hopefully, inspire new directions for future experimental research.

6.1. Ioffe time

It was first observed in QED [73] that photon emission from electrons propagating through a medium occurs over distances which increase with energy. In their seminal paper [74] Gribov, Ioffe and Pomeranchuk demonstrated that at high energies large longitudinal distances, now usually referred to as coherence-lengths, l_c , become important for any kind of projectile, including virtual photons, when considered in the

rest frame of the target. The typical time involved is $\mathcal{O}(E/\mu^2)$, with E the energy of the projectile and μ a hadronic mass scale, and basically follows from relativity. For DIS, Ioffe [75] demonstrated that the longitudinal distances involved, measured in the target rest frame and in the Bjorken limit, are growing as

$$l_c \propto \frac{1}{m_N x}, \quad (44)$$

where m_N is the target mass. It should be noted, however, that scaling violations, which are especially strong at small x , modify equation (44) and reduce the value of l_c [76]. In addition l_c depends on the polarization of the virtual photon.

The value of l_c becomes large for small x or large W . At HERA, for $Q^2 = 10 \text{ GeV}^2$, the x values range between 10^{-2} and 10^{-4} and l_c corresponds to distances of up to 1000 fermi. Pictorially speaking this means that partonic fluctuations of the virtual photon, the Fock states, are long-lived and travel a substantial distance before interacting.

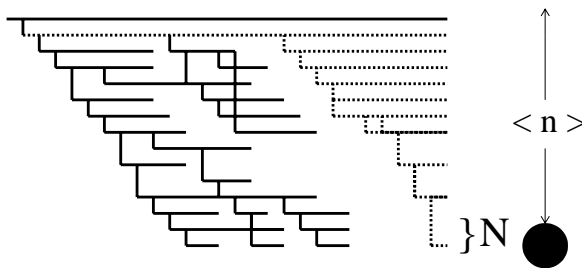


Figure 21. A high energy interaction in the parton model. From [67].

6.2. The Gribov-Feynman parton model

The parton model views a high-energy interaction of any projectile, particle a, with a target, particle b *at rest* as follows (see figure 21). The fast hadron fluctuates into point-like partons: quarks and gluons. The fluctuations have a lifetime $t \propto \frac{E}{\mu^2}$ before interaction with the target occurs. During this time the partons are in a coherent state which can be described by means of a wave function. Each parton can, in turn, create its own parton cascade, each creating $\langle n \rangle$ partons, resulting eventually in the emission of a total of N soft partons (“*wee*” partons in Feynman’s terminology [71]). The latter should not be confused with the partons of pQCD. They are non-perturbative (“dressed”) objects due to the long time-evolution of the cascade and have acquired a large transverse extension. They interact with a target with a large hadron-like cross section.

For a highly virtual photon, the cascade starts with a $q\bar{q}$ fluctuation (or dipole) of small transverse extension and is followed by an initial evolution stage where the strong coupling remains perturbative and calculable. However, the non-perturbative end of the cascade is likely to be similar to that originating from a high-energy hadron.

Since gluons rather than quarks will be the dominant component of the cascade, and since gluons carry a larger color charge, it should not have been a surprise to find that the interaction, when viewed in an infinite-momentum frame, is driven by the gluon constituents in the proton. The same holds for “diffractive” structure functions of the proton or of the Pomeron.

As argued by Gribov [72], a fast projectile can interact with the target only through its wee component. Indeed, the cross section of interaction of two point-like particles with large relative energy, $\sqrt{s_{ab}}$, is not larger than $\pi\lambda^2 \sim 1/s_{ab} \sim \exp(-\eta_{ab})$ (λ is the wavelength in the c.m. frame of a, b , η_{ab} is the relative rapidity). Thus, *only slow partons of the projectile* are able to interact with a non-negligible cross section. Since there are N wee partons in total, the interaction cross section is proportional to the probability that *at least one* wee out of N interacts with the target. For small N this is proportional to N .

The interaction can also be viewed from the rest-frame of the projectile, or from any collinear rest-frame. The distribution of the wee partons in the rest-frame of particle b is, according to the above arguments, solely determined by particle a and does not depend on the properties of particle b . On the other hand, in the rest frame of particle a the distribution is determined by the properties of particle b . This is possible only if the distribution of partons with rapidities η much smaller than the hadron’s rapidity, η_p , *does not* depend on the quantum numbers and the mass of that hadron. It follows that *the distribution of the wee partons with $\eta \ll \eta_p$ should be independent of the projectile and target*, i.e. be “universal”. Indeed, in the cascade the memory of the initial state is lost after a few steps only, if it resembles a Markov process.

The fact that the wee-parton component of any hadron is independent of the hadron itself, explains semi-qualitatively why hadronic total cross sections show a “universal” energy-dependence at large s , as discussed in section 3.1. In addition, if the interaction between wees is effectively short-range in rapidity (implying that the produced hadrons show short-range rapidity correlations), hadrons produced in regions of rapidity sufficiently far from target and projectile will also show “universal” properties.

6.2.1. Shrinkage. Consider the interaction in the impact-parameter plane, figure 2. In each step of the cascade the newly emitted parton acquires a certain amount of transverse momentum, k_T . If the emission is purely random in k_T -space, the last parton in the cascade will, as the result of a random walk in impact-parameter space, have moved a distance b_N^2 from the origin. On average, and for a completely random process (*which precludes any kind of p_T -ordering of the emissions*), one has

$$\langle b_N^2 \rangle \propto \frac{1}{\langle k_T^2 \rangle} N = \frac{\omega_0}{\langle k_T^2 \rangle} \ln s/s_0, \quad (45)$$

for $N \propto \ln s$. In this simplified picture, the (transverse) growth of the interaction region with energy is thus the result of a diffusion process. It is represented as the shaded area

in Fig. 2. Thus, $\omega_0/\langle k_T^2 \rangle$ can be identified with α'_P in equation (14). The argument based on the overlap function, section 5.1, leads to the same result but is more general.

It is superfluous to mention that wee-parton properties, and their interactions, cannot be calculated in pQCD, neither for hadronic collisions nor for deep-inelastic ep scattering, since they are associated with long-wavelength fluctuations of the color fields. For DIS, this ignorance is parameterized in the parton distributions at a small scale. However, in the small- x region, the wee partons are equally important in both types of scattering processes.

6.2.2. Rise of the total cross section and $\alpha_P(0)$. Consider figure 21. Since each parton in the parton cascade can form its own chain of partons, and so on, this multiplication process will generically (but not in detail) lead to a total mean $N \sim e^{\langle n \rangle}$, if $\langle n \rangle$ is mean multiplicity in a single chain [67]. With $\langle n \rangle \propto \omega_0 \ln s$ one finds:

$$N \propto s^{\omega_0}. \quad (46)$$

This can be rewritten in a frame-independent form

$$\sigma_T = \sigma_0(\text{projectile}) \times \sigma_0(\text{target}) \times \frac{1}{s_0} \times \left(\frac{s}{s_0} \right)^{\omega_0}. \quad (47)$$

The ‘‘impact-factors’’, σ_0 , are particle-specific but independent of s . Equation (47) ‘‘explains’’ the power-law (or Regge) behaviour of σ_T .

For a collision of a small-size (in b -space) virtual photon with a proton, Q^2 larger than a few GeV^2 , the evolution of ω_0 with Q^2 is calculable in pQCD. This is one of the major theoretical advantages of deep-inelastic scattering over soft hadron-hadron interactions. Evidently, in DIS, the role of s is taken over by W^2 or $1/x$.

From equation (47) we see again that $\alpha_P(0) - 1$ in Regge theory has to be interpreted as the wee-parton density in a parton cascade. This result is generic. However, since the detailed process-specific dynamics of the parton cascade (DGLAP [77], BFKL [78],...) will influence the evolution of ω_0 , we may conclude that a ‘‘universal’’ Pomeron trajectory with process-independent parameters does not exist.

The power-law form, equation (47), is a result typical for a self-similar (fractal) branching process with *fixed coupling constant* and ω_0 is related to the fractal dimension. Early pre-QCD examples can be found in [79]. For a running coupling constant, the s dependence is generally less strong, but faster than any power of $\ln s$.

6.2.3. Total cross sections, diffraction and wee-parton multiplicity. Suppose the projectile is a superposition of states with, at given impact parameter b , n wee partons, each of which can interact with the target with a probability $f(b)$. If the structure of the target is ignored, we have (for brevity, we omit the argument b in the following)

$$\sigma_{tot} = \sum \sigma_{tot}(n)P(n); \quad (48)$$

where $P(n)$ is the probability that the cascade has produced n such partons. Using conservation of probability (or unitarity) we find

$$\sigma_{tot}(n) = 2T_{el}(n); \quad T_{el}(n) = 1 - \sqrt{1 - \sigma_{in}(n)}; \quad \sigma_{in}(n) = 1 - (1 - f)^n. \quad (49)$$

The last equation in (49) is the probability that *at least one* out of n partons interacts with the target.

The previous equations can be compactly expressed in terms of the generating function of $P(n)$, $\Xi(z)$

$$\Xi(z) = \sum P(n) (1+z)^n, \quad (50)$$

$$\sigma_{tot} = 2 \sum P(n) [1 - (1-f)^{n/2}] = 2 - 2\Xi(\sqrt{1-f} - 1), \quad (51)$$

$$\begin{aligned} \sigma_{diff+el} &= \sum P(n) [1 - (1-f)^{n/2}]^2, \\ &= 1 - 2\Xi(\sqrt{1-f} - 1) + \Xi(-f). \end{aligned} \quad (52)$$

For the ratio of total diffractive (sum of inelastic and elastic) cross section to the total cross section, $R(b)$, at fixed impact parameter, we obtain

$$R(b) = \frac{\sigma_{diff+el}}{\sigma_{tot}} = 1 - \frac{1}{2} \frac{1 - \Xi(-f)}{1 - \Xi(\sqrt{1-f} - 1)}. \quad (53)$$

In the case of total absorption, $f \rightarrow 1$, the ratio converges towards the black-disk limit of $\frac{1}{2}$, as it should⁺.

Assuming, as an example, $P(n)$ to be Poissonian we obtain

$$\sigma_{tot} \approx \frac{1}{2} f \langle n \rangle, \quad (54)$$

$$\sigma_{diff+el} \approx \frac{f^2}{4} \langle n^2 \rangle = \frac{f^2}{4} [\langle n \rangle^2 + \langle n \rangle]; \quad (55)$$

provided f or $\langle n \rangle$ or both are small enough. These conditions mean that multiple interactions with the target can be neglected, or that the partonic system hitting the target is sufficiently dilute and no saturation takes place.

Equation (54) suggests a relation between the total cross section (or F_2 in DIS) and the mean parton multiplicity which was first tested experimentally in [80] and is illustrated in Fig. 22. Using a Modified Leading Log (MLLA) pQCD expression for the energy-dependence of $\langle n \rangle$ (Eq. (7.32) in [81]), an excellent description of the x -dependence of $F_2(x, Q^2)$ data at low x was achieved with two free parameters only.

If saturation (parton-recombination) effects in the parton cascade in DIS happened to occur, we can expect that the similarity of the energy-dependence between mean particle multiplicities in e^+e^- and F_2 will break down for very high multiplicity events. Given the present interest in this topic [28], a dedicated measurement of the W -dependence of semi-inclusive structure functions $F_2^{(n)}(x, Q^2)$, at fixed large final-state multiplicity n , and of its diffractive counterpart, might therefore be of considerable importance.

Assuming a s^ϵ dependence of $\langle n \rangle$, we further see that (54) and (55) predict the energy-dependences $\sigma_{tot} \propto s^\epsilon$ and $\sigma_{diff+el} \propto s^{2\epsilon}$, the same as obtained in Regge theory,

⁺ For DIS at very large W , it follows, quite remarkably, that for scattering on a very large fully absorbing nucleus, 50% of the total cross section will be diffractive, even when Q^2 is very large (but $Q^2/W^2 \ll 1$).

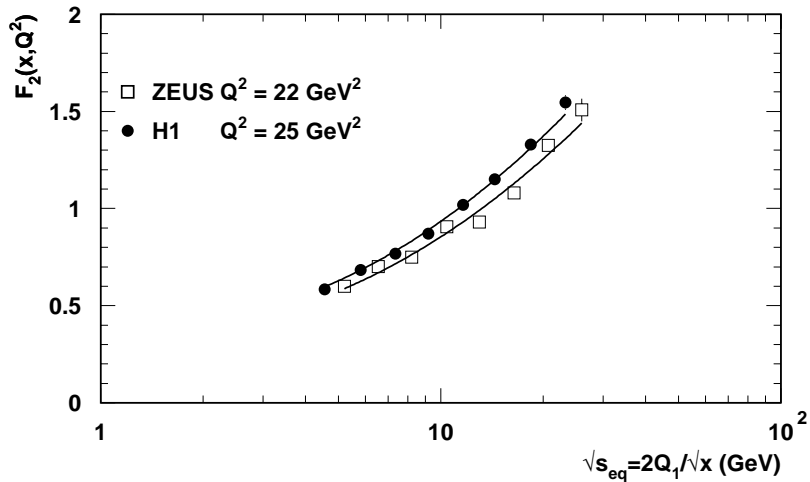


Figure 22. Comparison of e^+e^- data on average charged particle multiplicities versus \sqrt{s} and the HERA low- x F_2 data versus $2Q_1/\sqrt{x}$, with $Q_1 = 270$ MeV, for $Q^2 = 22$ GeV 2 (ZEUS) and 25 GeV 2 (H1). The e^+e^- multiplicity data (solid lines) are represented by curves resulting from a phenomenological fit of a second-order polynomial in $\ln s$ to e^+e^- data. They are normalized to the F_2 data for each Q^2 bin separately. From [80].

and thus show the same unitarity violating defects as mentioned in section 2.2.3. To obtain a constant ratio, $R(b)$, at each impact parameter, it seems unavoidable to include in the calculation the full multiple-scattering terms and possibly (so far unknown) parton correlations.

The role parton correlations can be illustrated using the factorial cumulant expansion of $\Xi(z)$ (see e.g. [82, 83]):

$$\Xi(z) = \exp \left\{ \langle n \rangle z + \sum_2^{\infty} (z^q/q!) K_q \right\},$$

The cumulants K_q are a measure of the correlations and identically zero for $q > 1$ if the partons are uncorrelated. The inelastic cross section can now be written as

$$\sigma_{\text{in}} = 1 - \Xi(-f) = 1 - \exp \left\{ -Nf + \sum_{q=2}^{\infty} (-f)^q/q! K_q \right\}. \quad (56)$$

Comparing equation (32) with equation (56) we see that the eikonal function $\Omega(b)$ can be expressed in terms of the cumulant generating function $\ln \Xi(-f)$. This shows that not only multiple scattering contributions, but also parton-parton correlations (provided that $K_q \neq 0$ for $q > 1$) contribute to the total and diffractive cross sections. Such correlations have not been explicitly taken into account, as far as we know, in present pQCD calculations of DDIS, with the exception of [84] using the concept of (Mueller) dipoles in onium-onium scattering.

6.3. Models for diffraction

6.3.1. Diffraction and the parton model: the Miettinen and Pumplin paper. The first detailed calculations of hadronic diffraction in the framework of the parton model were presented in [85]. This work, although 22 years old, remains of great interest and we summarize its main conclusions.

It is assumed that the diagonal states (section 5.2) $|\Psi_k\rangle$ are the states of the parton model, composed of quarks and gluons and a radiation cloud of wee partons. These states are characterized by a definite number N of partons with impact parameters $\vec{b}_1, \dots, \vec{b}_N$ and longitudinal momentum fractions, or rapidities, y_1, \dots, y_N .

Since there are parton states which are rich in wee partons, and others with a few or no wees, these states will interact with a target with very different cross sections. Hence, inelastic diffraction will be generated by the mechanism of Good and Walker. The fluctuations in the interaction probabilities t_k (equation (39)) arise from fluctuations in the number of wee partons, fluctuations in y_i and from fluctuations in \vec{b}_i .

Assuming uncorrelated wee partons, and fitting all free parameters of the model to $\sigma_{\text{el}}(pp)$ and $\sigma_{\text{T}}(pp)$ at $\sqrt{s} = 53$ GeV, the calculated total inelastic diffractive cross section was found to be in very good agreement with data. The y_i fluctuations contribute little (about 10%), whereas fluctuations in b_i and in parton number each account for about 45% of $\sigma_{\text{in}}^{\text{DD}}$. Also the forward value and the slope of the t distribution are correctly predicted. This is a non-trivial result since the calculated (and measured) slope $B \approx 6.9$ GeV⁻² is only about half that of elastic scattering $B \approx 12$ GeV⁻². Interestingly, as seen from figure 23, the small $|t|$ dissociation is dominated by the large and very steep (slope ≈ 12.2 GeV⁻²) contribution due to the parton-number fluctuations, see also equation (55). The b_i fluctuations, on the other hand, dominate at large $|t|$.

The ZEUS collaboration recently presented new measurements, shown in figure 24 (see [86]), of the t -slope in diffractive DIS, using their Leading Proton Spectrometer (LPS). The slope has a value $B = 6.8 \pm 0.6$ (stat) $_{-0.7}^{+1.2}$ (syst) for $4 < Q^2 < 100$ GeV², $M_X > 2$ GeV, $\xi < 0.03$. Some evidence for shrinkage is seen but no dependence on Q^2 . The value of the t slope is strikingly similar to that in the pp data.

6.3.2. Modern QCD models of diffraction It is evident that the Miettinen-Pumplin (MP) model grasps the essential physics which remains valid in the context of DDIS at HERA. In [85] ad-hoc assumptions were needed to build a model of the hadron Fock states. In DIS the light-cone “wave functions” of the lowest-order γ^* Fock states ($q\bar{q}$, $q\bar{q} + \text{gluon}$) are known [49, 87] and quantitative results can be obtained. Nevertheless, the interaction of the wee partons needs to be parameterized empirically, as it must be for soft hadron-hadron collisions.

The presently popular models for diffraction in DIS have been reviewed in [2]. They use the same basic concepts discussed in previous sections under various disguises. The most successful of these are merely modernized versions of the Aligned Jet Model [49]

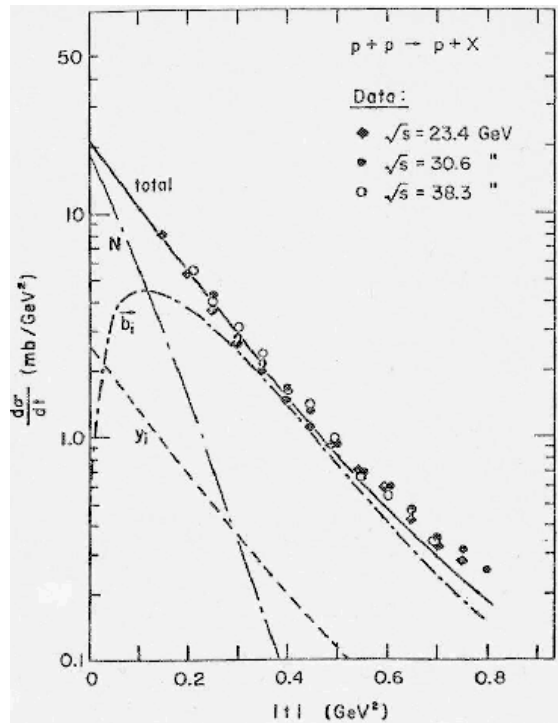


Figure 23. Differential t distribution, $\frac{d\sigma^{DD}}{dt}$, and model calculations. The decomposition is shown of the full cross section into contributions due to fluctuations in the number (N), rapidities (y_i) and relative impact parameters (b_i) of the wee partons. The N -fluctuation dominates near $t = 0$, and the b_i fluctuation component at large t . From [85].

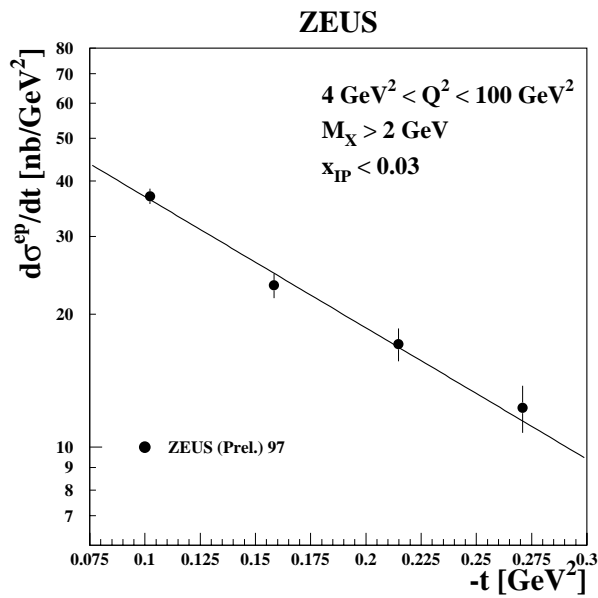


Figure 24. ZEUS: the t distribution measured in DIS, using the Leading Proton Spectrometer [86]. The slope has a value $B = 6.8 \pm 0.6$ (stat) $^{+1.2}_{-0.7}$ (syst)

which pre-dates QCD.

Considered in the target rest frame, the Fock-state wavefunction of the partonic γ^* fluctuation carries the information on the virtuality of the photon and further depends on its transverse size and the fractional momenta and masses of the partons. In the simplest case of a $q\bar{q}$ fluctuation, or $q\bar{q}$ dipole, the wave function is then convoluted with the amplitude for the elastic interaction of the colour dipole and the target hadron. At $t = 0$, this amplitude is determined by the cross section for the scattering of the dipole with the target, $\sigma(\varrho)$. It is assumed to be independent of Q^2 , in accord with the Gribov-Feynman argument of wee-parton scattering and short-range order in the cascade, but depends on x .

Consider, as an example, the very successful saturation model of Golec-Biernat and Wüsthoff (GBW) [28] which expands on much earlier work [87]. The physical picture is that in which, in the nucleon rest frame, a photon with virtuality Q^2 , emitted by a lepton, dissociates into a $q\bar{q}$ pair far upstream of the nucleon. This is then followed by the scattering of the colour dipole on the nucleon. In this picture, as also assumed in the MP model, the relative transverse separation ϱ of the $q\bar{q}$ pair and the longitudinal momentum fraction z of the quark remain essentially unchanged during the collision. The γ^*p cross sections take the following factorized form [87, 88]

$$\sigma_{T,L}(x, Q^2) = \int d^2\varrho \int_0^1 dz |\Psi_{T,L}(z, \varrho, Q^2)|^2 \sigma(x, \varrho), \quad (57)$$

where $\Psi_{T,L}$ is photon wave function of transversely (T) and longitudinally polarized (L) photons.

In (57), all Q^2 dependence is contained in the Fock-state wavefunction, which further depends on the flavour and mass of the partons. The W - or x -dependence of $\sigma_{T,L}(x, Q^2)$ is solely determined by that of $\sigma(x, \varrho)$. The latter is the principal quantity in the s -channel description of diffractive scattering. Once the dipole cross section is known, (57) enables a parameter-free calculation of the proton structure function at small x . In our simple picture, we may interpret it as an effective cross section, the product of the wee-parton flux with the single wee-parton nucleon cross section.

Although the impact-parameter dependence of $\sigma(x, \varrho)$ is not explicitly considered (only its average enters in (57)), this is clearly of great interest for the t -dependence of the diffraction [69], and needs to be studied further.

Turning to diffraction, the differential cross section at $t = 0$ takes the form

$$\left. \frac{d\sigma_{T,L}^D}{dt} \right|_{t=0} = \frac{1}{16\pi} \int d^2\varrho \int_0^1 dz |\Psi_{T,L}(z, \varrho)|^2 \sigma^2(x, \varrho). \quad (58)$$

The form of (58) differs only from (57) by the substitution $\sigma(x, \varrho) \rightarrow \sigma^2(x, \varrho)$, in accord with the general formula (42) *.

* In the dipole formulation of DIS, and contrary to hadron diffraction, even inelastic DDIS is considered to be purely elastic: the dipole states ($q\bar{q}$) and higher-order Fock-states $q\bar{q} + \text{gluons}$ are assumed to be orthogonal eigenstates of the diffractive T -matrix, and no regeneration (mixing of the states) occurs. If these states are not orthogonal, they will regenerate and thus add an additional contribution to the

Comparing to the MP-model, we see that the relative impact parameter and rapidity fluctuations are included here through the photon wave function. The important parton-number fluctuations, which also depend on parton-parton correlations, however, are not explicitly considered.

The energy-dependence of $\sigma(x, \varrho)$ follows from the fact that, in low- x DIS, the perturbative evolution of the $q\bar{q}$ dipole results in further “hard” parton multiplication which increases also the wee-parton flux and thus the total cross section. Indeed, due to the bremsstrahlung nature of soft gluon spectrum $\propto dz_g/z_g$ (z_g is the momentum fraction of the photon carried by a gluon) Fock states with n such gluons give a contribution $\propto \ln(1/x)^n$ to the total photoabsorption cross section, which can be reabsorbed into an energy-dependent dipole cross section [87]. For example, in the DGLAP approximation, summing over all n produces the well-known $\exp[2\sqrt{\ln(1/x)\ln(1/\alpha_s(Q^2))}]$ increase of the γ^*p cross section and “standard” scaling violations.

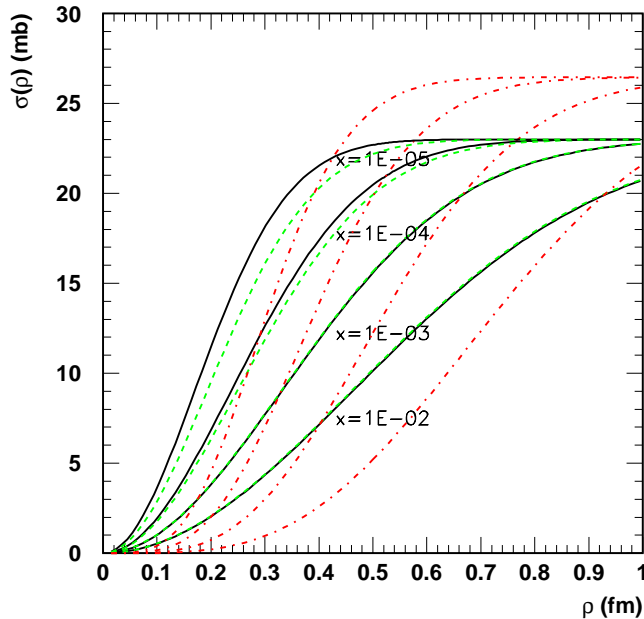


Figure 25. The dipole cross section $\sigma(\varrho)$ for various values of Bjorken- x . The GBW parameterisation, Eqs. 60 and 61, with $\lambda = 0.29$ is shown as the solid curve. The dashed lines correspond to the $1/x$ dependence given by Eq. 62 with parameters $n_f = 3$, $K = 0.288$, $\Lambda = 1.03$ GeV, taken from [89]. The dot-dashed lines show $0.05 \times \sigma^2(\varrho)$.

The $q\bar{q}$ dipole-proton cross section $\sigma(x, \varrho)$ has to be modelled although it is known in the perturbative limit of very small dipoles and related there to the inclusive gluon diffractive cross section, presently neglected.

distribution $xg(x, \mu^2)$ of the target [90].

$$\sigma(x, \varrho) = \frac{\pi^2}{3} \alpha_s [xg(x, C/\varrho)] \varrho^2 + \mathcal{O}(\varrho^4), \quad (59)$$

valid at small ϱ ; C is a scale parameter. For a $(q\bar{q}g)$ -dipole system, $\sigma(x, \varrho)$ is roughly a factor 9/4 larger. This explains the predominant role of gluons in low- x DIS. In the GBW model, the effective dipole cross section is taken to be of the form

$$\sigma(x, \varrho) = \sigma_0 \left[1 - \exp\left(-\frac{\varrho^2}{4R_0^2(x)}\right) \right], \quad (60)$$

where the x -dependent radius R_0 is parameterized as

$$\frac{1}{R_0^2(x)} = Q_0^2 \left(\frac{x_0}{x}\right)^\lambda, \quad (61)$$

with $Q_0 = 1$ GeV. The parameters $\sigma_0 = 23$ mb, $x_0 = 3 \cdot 10^{-4}$ and $\lambda = 0.29$ have been determined by a fit to data on F_2 [28]. As seen in figure 25, the dipole cross section saturates at a value σ_0 for large-size dipoles where it is entirely non-perturbative. Also, as $x \rightarrow 0$, saturation sets in at decreasingly small transverse sizes, and the contribution from large-size dipoles becomes more important.

Since equation (58) depends on the square of $\sigma(x, \varrho)$, it follows that still larger sizes are involved in diffraction than those dominating the total cross section: non-perturbative soft physics is of even greater importance in DDIS (see the dot-dashed lines in Fig. 25). Saturation effects are therefore predicted to be more important than in inclusive DIS. Because of the saturation property of (60), nearly the same dependence on x and Q^2 of DDIS and DIS is found, thus giving a natural explanation of the constancy of their ratio as mentioned in section 4.3.

In the GBW model, two essential scales appear: the characteristic transverse size of the $q\bar{q}$ dipole $\propto 1/Q$, solely determined by the γ^* wave function, and $R_0(x)$. Naively, $1/R_0^2(x)$ can be interpreted as the mean number of soft partons in the cascade; $R_0(x)$ is their mean relative transverse distance and $Q R_0(x) = 1$ defines a critical line. For $1/Q \ll R_0(x)$ the partonic system is dilute, for $1/Q \gg R_0(x)$ the system is densely packed and multiple scattering and parton-interactions become important.

It is interesting to note here that the fitted value of λ (≈ 0.29) is quite close to that derived from the c.m. energy-dependence (\sqrt{s}) of the mean particle multiplicity in e^+e^- annihilation, where it is found that $\langle n \rangle \sim s^{0.25}$ provides a reasonable fit of the data [91]. Remembering the striking analogy discussed in section 6.2.3, we have also plotted in figure 25 expression (60) wherein $1/R_0^2(x)$ in Eq. (61) is replaced by that of the mean soft gluon multiplicity in a gluon jet with energy-squared $\propto 1/x$, as given in [89]

$$\frac{1}{R_0^2} \equiv Q_0^2 N_g = K Q_0^2 y^{-a_1 C^2} \exp[2C\sqrt{y} + \delta_G(y)], \quad (62)$$

with K an overall normalization constant, $C = \sqrt{4N_c/\beta_0}$, and

$$\delta_G(y) = \frac{C}{\sqrt{y}} \left[2a_2 C^2 + \frac{\beta_1}{\beta_0^2} [\ln(2y) + 2] \right] + \frac{C^2}{y} \left[a_3 C^2 - \frac{a_1 \beta_1}{\beta_0^2} [\ln(2y) + 1] \right]. \quad (63)$$

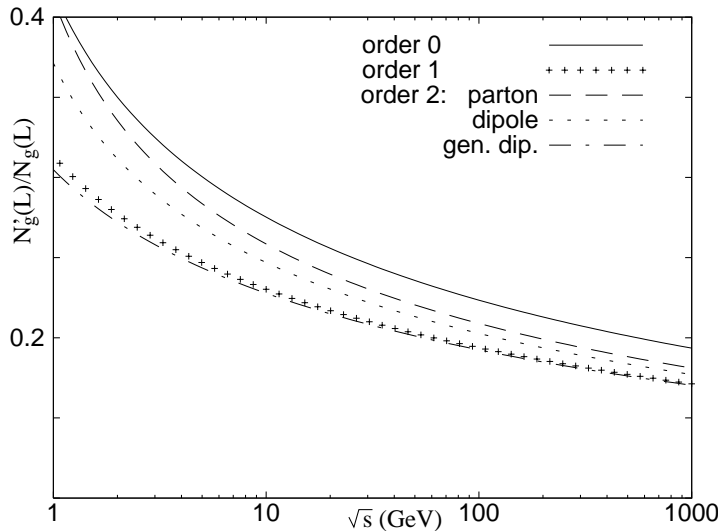


Figure 26. Anomalous multiplicity dimension to different orders in $\sqrt{\bar{\alpha}}$. The chosen example is $N_f = 4$ and $\Lambda = 0.22$ GeV. Anomalous dimension N'_g/N_g as $\bar{\alpha} = 3\alpha_s/2\pi$ (solid line), $\sqrt{\bar{\alpha}}(1-2a_1\sqrt{\bar{\alpha}})$ (crossed) and $\sqrt{\bar{\alpha}}(1-2a_1\sqrt{\bar{\alpha}}-4a_2\bar{\alpha})$ for the parton equation (dashed), dipole equation (dotted) and generalized dipole equation (dash-dotted). The constants are $a_1 = 0.297$, $a_2 = -0.339$. For a detailed discussion see [93].

Here $e^y = \sqrt{1/x}/\Lambda$ and further $\beta_0 = (11N_c - 2n_f)/3$, $\beta_1 = [17N_c^2 - n_f(5N_c + 3C_F)]/3$, $N_c = 3$ is the number of colours and $C_F = 4/3$. The numbers a_i are tabulated in [92]. Λ is the QCD scale parameter and n_f the number of active flavours.

The dashed curves in figure 25 show the dipole cross section as obtained from equation (62). It is essentially indistinguishable from the GBW parameterisation for $x = 10^{-2} - 10^{-3}$, but differences become noticeable at smaller x . This follows from the fact that, due to the running of α_s , the multiplicity grows slower than a power in $1/x$ and “saturation” is delayed in comparison with Eq. (61), the latter being a result characteristic of a cascade process with a fixed coupling constant.

The results shown in Fig. 25 imply that the ansatz in Eq. (62) will lead to an equally satisfactory description of F_2 and F_2^D as was obtained in the original GBW work. However, the parameterization (62), contrary to (61), involves no free parameters, apart from Q_0 and the normalization constant K which was taken from a fit to e^+e^- data [89]. In particular, the important parameter λ follows in the former case from theory.

If $1/R_0^2(x)$ is interpreted as the mean number of soft partons confined in the target within a transverse surface of radius R , it is evident that the GBW parameter λ can be identified with the anomalous (multiplicity) dimension, $\tilde{\gamma}$, of the parton cascade (see [94] for a recent review and further references) which is calculable in pQCD.

With $L = \ln(s/\Lambda^2)$ (s is the relevant energy-scale squared, $1/x$ for DIS), $\tilde{\gamma}$ is in general defined as

$$N_g \propto \exp \left[\int_{y_0}^y \tilde{\gamma}(y') dy' \right]. \quad (64)$$

where N_g is the mean gluon multiplicity. In pQCD, for a time-like cascade, it is equal to the logarithmic derivative of N_g with respect to L and given by [89]

$$\tilde{\gamma} = \frac{N'_g(L)}{N_g(L)} = \sqrt{\bar{\alpha}} (1 - 2a_1\sqrt{\bar{\alpha}} - 4a_2\bar{\alpha} + \mathcal{O}(\bar{\alpha}^{3/2})) \quad (65)$$

The first term, $\sqrt{\bar{\alpha}} \equiv \sqrt{N_c\alpha_s/2\pi}$, is the leading-order term. However, $\tilde{\gamma}$ is non-linear in $\bar{\alpha}$ and decreases with increasing s . Figure 26 shows a plot of the anomalous dimension, calculated to different orders in $\bar{\alpha}$ and for various cascade schemes (parton-cascade and Lund-dipole pictures) as discussed in [93]. It is seen that $\tilde{\gamma}$ decreases with s due to the running of α_s . Consequently, N_g increases slower than a power of s . A power-law dependence is obtained if α_s is kept constant. Taking, as an example, $\alpha_s = 0.2$ in (65) yields $\lambda = 0.30$ at lowest order.

The relation between the GBW parameter λ and the multiplicity anomalous dimension has also been derived in the framework of the Balitsky and Kovchegov modified BFKL equation (see [95] for details and references) with the result $\lambda \approx 6\alpha_s/\pi$. For $\alpha_s = 0.2$ this gives $\lambda = 0.38$. Note, however, that (65) is a polynomial in $\sqrt{\bar{\alpha}_s}$, whereas the previous expression is linear in α_s .

An further important result of the GBW-model is that the diffractive structure function F_2^D is found to obey a Regge-like factorization property (except for $\beta \rightarrow 1$ where higher-twist contribution from longitudinal photons dominate) with the dependence $F_2^D \propto (1/\xi)^{1+\lambda}$. This corresponds to an effective Pomeron intercept $\alpha_{\mathbb{P}}(0) \sim 1 + \lambda/2$ [96]. This is a highly revealing result, demonstrating, on this specific model-example, the generic property that the growth of the cross sections with energy and the proton energy-loss spectrum (or ‘‘Pomeron flux’’) are closely connected (cfr. section 4.3.1) and determined by the multiplicity anomalous dimension.

The above considerations suggest an extremely simple picture (see also [97] p.8) for the x and Q^2 dependence of F_2 and F_2^D . At low x , the target is populated with a number of partons proportional to N_g confined within a transverse area πR^2 . Since the area ‘‘scanned’’ by the virtual photon $q\bar{q}$ dipole is proportional to $1/Q^2$, the number of partons with which it can interact is proportional to $\frac{1}{\tau} \equiv N_g \frac{1}{Q^2} \propto \frac{1}{R_0^2} \frac{1}{Q^2}$. One can therefore expect that the total cross section will depend only on τ and not on Q^2 and R_0^2 separately, i.e. exhibit ‘‘geometrical scaling’’ [98]. This follows already from dimensional arguments but also agrees with the ‘‘universality’’ hypothesis, advanced in [99], that the physics should depend only on the number of partons per unit of rapidity and per unit of transverse area. If $1/\tau$ is sufficiently small, multiple scattering effects can be neglected.

To see the influence of multiple scattering, we return to formulae (51)-(52) which we now apply to the cross section of a dipole of fixed size ϱ interacting with the target. We further assume that parton correlations can be neglected. In that case, the generating function $\Xi(z)$ is that of a Poisson distribution $\Xi(z) = \exp(\langle n \rangle z)$. Provided that f is small enough we obtain

$$\sigma_{tot}^{dipole} \simeq 2 \left(1 - e^{-\frac{1}{2}\langle n \rangle f} \right) \quad (66)$$

$$\sigma_{diff+el}^{dipole} \simeq 1 - 2 e^{-\frac{1}{2}\langle n \rangle f} + e^{-\langle n \rangle f} \quad (67)$$

Equation (66) is precisely of the GBW (eikonal) form (60) if, following the previous arguments, $\langle n \rangle_f$ is identified with $1/\tau$, the effective number of partons “seen” by the $q\bar{q}$ dipole.

The above formulae invite further comments on the meaning of the term “saturation”. The form of equation (66) follows from that of the generating function which includes the full Glauber-Mueller multiple scattering series which leads to a levelling off of the dipole cross section. Only for a very dilute parton system, or for a very small dipole can these additional terms be neglected. On the other hand, parton recombination effects, when they occur, will induce a weaker $1/x$ dependence of $\langle n \rangle$, compared to that given e.g. by Eq. (62). Although our simple semi-classical picture therefore suggests *two distinct origins* of saturation, it is not clear if such a distinction is physically justified in more rigorous treatments of the dynamics.

The model results, discussed previously in the target rest frame, can be translated, at least in leading twist, in terms of diffractive parton densities in an infinite momentum frame. The diffractive structure functions are then expressed as the convolution of “diffractive” parton densities *for the proton* with parton cross sections [100]. The evolution with Q^2 at fixed x is the same as that of $F_2(x, Q^2)$. In DDIS, these scaling violations affects the β (or M_X) dependence of the cross section but not the dependence on ξ . However, unlike the case of fully inclusive cross sections, the diffractive structure functions are no longer universal. In particular, they cannot be used directly for hadronic interactions [96].

7. Summary and outlook

Over the last decade, the subject of diffraction has become one of the very active fields of experimental and theoretical research in QCD. The revival is, by large, due to the extremely varied experimental programme made possible at HERA and at the Tevatron.

In this paper, we have attempted to describe, mainly in qualitative terms, the close relation between the dynamics of total cross sections and diffraction in hadron-hadron collisions and in deep-inelastic γ^*p scattering. This inter-relationship is ultimately a consequence of the fact that the bulk of the total and diffractive cross section is dominated at very high energy by the wee components of the target and projectile’s wavefunctions such that long-distance physics plays a very important role in both.

We have argued that the physics can be understood on the basis of a surprisingly small number of dynamical ingredients such as the anomalous multiplicity dimension of parton cascades, $\tilde{\gamma}$, which not only determines the rise with energy of the cross sections but also the spectrum of the elastically scattered proton in DDIS.

Our discussion of the overlap function illustrates that the small $|t|$ behaviour of the quasi-elastic processes is also determined by $\tilde{\gamma}$ and by the transverse-momentum transfer correlation function. These ingredients suffice for a basic understanding of the degree of “shrinkage” of the forward diffractive peaks in soft as well as in hard processes.

The remarkable recent theoretical progress in DDIS is a consequence of the

fortunate circumstance that perturbative QCD is able to make reliable predictions for the partonic fluctuations (Fock states) of a virtual photon, and for the subsequent development of these states into a parton shower or radiation cloud, at least in the earliest perturbative phase of the evolution. For a strongly bound system of large size, e.g. a hadron, which is less well understood, such perturbative techniques are not available.

Much of the present phenomenology of diffraction can be understood from the properties of the γ^* Fock states.

- The M_X distribution for the lowest-order $q\bar{q}$ dipole state, and transversely polarized γ^* , has the form $1/[m_f^2(Q^2 + M_X^2)]$ (m_f is the quark mass). Extra soft gluon emission, with a spectrum dz_g/z_g directly leads to the much weaker M_X dependence $dM_X^2/(M_X^2 + Q^2)$ in the so-called triple-Pomeron region [87]. Since the invariant mass of the diffractive system will remain almost unchanged for small- t scattering, this is also the distribution of the experimentally measured M_X . A similar argument was used in [57] to explain the $1/M_X^2$ dependence of hadronic diffraction at large M_X . The gradual transition from a steep $1/M_X^4$ to a $1/M_X^2$ dependence is a consequence of a change in the mixture of Fock states as Q^2 and/or W change.
- The average transverse size of γ^* fluctuations relevant for elastic vector meson production, the so-called scanning radius [39], is estimated to be $\sim C/(m_V^2 + Q^2)$, with $C \sim 2$ ($C \sim 6$) for longitudinally (transversely) polarized γ^* [69]. This follows almost directly from the form of $|\Psi_{T,L}|^2$ and from that of the vector-meson wavefunction. The elastic vector meson data (see e.g. figure 10 in section 3.3.2) show that scale $Q_{eff} = Q^2 + m_V^2$ is indeed the dynamically relevant observable. For further discussion on this point we refer to [52].
- For high-mass diffraction, the partonic fluctuation of the γ^* has the colour-topology of a gluon-gluon dipole in a colour-single state [87]. High-mass diffraction therefore opens the possibility, not yet fully exploited, to study the fragmentation of colour-octet sources, in much the same way as with $q\bar{q} +$ gluon three-jet events in e^+e^- annihilation.

The development of the radiation cloud initiated by the virtual photon is a cascade process, whereby the virtuality of the system is gradually degraded and a system of “perturbative” partons created. However, once the virtuality of the partons has reached values for which the strong coupling is no longer small, the cascade will continue into a non-perturbative region which is not under theoretical control. This corresponds to a regime in which the non-perturbative off-springs have acquired transverse dimensions comparable to the size of the target proton. It can be assumed that they will interact with the target as dressed objects, with a large hadron-like cross section. This and the variation in absorption is, by the mechanism of Good and Walker, the cause of shadow-scattering and diffraction, not only in DIS but also in hadron-hadron scattering.

At large energy, the end of the parton cascade will show “universal” properties, independent of the parton system which initiated the cascade. This, in turn, leads

to expect factorization of the type often assumed in Regge theory and also found experimentally.

The simple picture described here suggests further experimental work in different directions. We end by listing only a few examples.

- Studies of leading-proton and leading-neutron production in DIS and photoproduction, also outside the diffractive region, combined with the many existing hadron-hadron data, should allow to test Regge-type factorization or provide evidence for factorization breaking. The latter is expected at low to moderate values of Q^2 . Evidence for possible long-range correlations between leading baryons and “central” hadronic activity (multiplicity, transverse energy density, jets) should be searched for.
- The running of α_s and $\tilde{\gamma}$, see Fig. 26, suggest to measure in detail the ξ dependence of $F_2^D \sim (1/\xi)^{1+\lambda}$ as function of W and Q^2 . Whereas the kinematical range of the HERA experiments may be too limited to reveal an expected flattening of the $d\sigma/dM_X^2$ spectrum, running- α_s and possible parton saturation effects which affect the value of λ may become visible at LHC energies.
- Since parton saturation is most likely to occur for high parton densities, a dedicated measurement of the W -dependence of semi-inclusive structure functions $F_2^{(n)}(x, Q^2)$, and of its diffractive counterpart, for large final-state multiplicity (n) events could of considerable interest.
- The dipole cross section $\sigma(x, \rho)$ plays a fundamental role in many models. At HERA, it can be measured in elastic vector-meson production but needs precise measurements of the differential cross section over a large range in t .

Acknowledgments

It is a pleasure to thank the organisers of the Ringberg Workshop on “New Trends in HERA Physics 2001” for a very stimulating meeting in a splendid environment. I further wish to thank A. Białas for interesting discussions which are partly reflected in section 6.2.3 and T. Anthonis, A. De Roeck, G. Lafferty and P. Van Mechelen for reading of the manuscript and helpful comments.

References

- [1] H. Abramowicz, A. Caldwell, *Rev. Mod. Phys.* **71** (1999) 1275; Abramowicz H, *Int. J. Mod.Phys.* **A15S1** (2000) 495; eConf C990809 (2000) 495.
- [2] Wüsthoff M and Martin A D, *J. Phys. G* **25** (1999) R309 [[hep-ph/9909362](#)]; Hebecker A, *Acta Phys. Pol. B* **30** (1999) 3777; *Phys. Rep.* **331** (2000); Buchmüller W, *Towards the theory of diffractive DIS*, talk presented at “New Trends in HERA Physics”, Ringberg Workshop, 1999, [[hep-ph/9906546](#)]; Hebecker A, *Phys. Rep.* **331** (2000) 1 [[hep-ph/9905226](#)].
- [3] Ingelman G and Schlein P, *Phys. Lett. B* **152** 1985 256.
- [4] Hebecker A, *Non-perturbative high-energy QCD*, Int. Europhysics Conf. on HEP, Budapest, 2001 [[hep-ph/0111092](#)].

- [5] Frautschi S C, Gell-Mann M and Zachariasen F, *Phys. Rev. D* **126** (1962) 2204.
- [6] Gribov V N, *JETP Lett.* **41** (1961) 667.
- [7] Pomeranchuk I Ya, *Sov. Phys. JETP* **34** (1958) 499.
- [8] Donnachie A and Landshoff P V, *Nucl. Phys. B* **231** (1984) 189.
- [9] Gaidot A *et al*, *Phys. Lett. B* **57** (1975) 389.
- [10] Mueller A H, *Phys. Rev. D* **2** (1970) 2963.
- [11] Brower R C and Weiss J H, *Rev. Mod. Phys.* **47** (1975) 605.
- [12] Froissart M, *Phys. Rev. D* **123** (1961) 1053; Lukaszuk L and Martin A, *Nuovo Cim. A* **52** (1967) 122.
- [13] Goulianos K and Montanha J, *Phys. Rev. D* **59** (1999) 114017.
- [14] ZEUS collab., Breitweg J *et al*, *Eur. Phys. J. C* **6** (1999) 43.
- [15] H1 Collab., *Measurement of diffractive structure function $F_2^{D(3)}$ at HERA*, EPS2001, abstract 808.
- [16] Donnachie A and Landshoff P V, *Phys. Lett. B* **296** (1992) 227.
- [17] Denisov S P *et al*, *Phys. Lett. B* **36** (1971) 415.
- [18] Amaldi U *et al.*, *Phys. Lett. B* **44** (1973) 112; Amendolia S R *et al*, *Phys. Lett. B* **44** (1973) 119.
- [19] Carroll A S *et al*, *Phys. Lett. B* **61** (1976) 303.
- [20] Cudell J R, *et al*, *Soft pomeron and lower-trajectory intercepts* [hep-ph/9812429]; Kang K *et al*, *Analytic Amplitude Models for Forward Scattering* [hep-ph/0111360].
- [21] Covelan R, Montanha J and Goulianos K, *Phys. Lett. B* **389** (1996) 176.
- [22] Dubovikov M S and Ter-Martirosyan K A, *Nucl. Phys. B* **214** (1997) 163.
- [23] Cudell J R *et al*, *Phys. Rev. D* **61** (2000) 034019; Erratum *Phys. Rev. D* **63** (2001) 059901.
- [24] Chliapnikov P V, Likhoded A K and Uvarov V A, *Phys. Lett B* **215** (1988) 417.
- [25] Abramovski V A, Gribov V N and Kancheli O V: *Sov. J. Nucl. Phys.* **18** (1974) 308.
- [26] Kaidalov A B, Ponomarev L A and Ter-Martirosyan, *Sov. J. Nucl. Phys.* **44** (1986) 468.
- [27] Martin A D, Roberts R G and Stirling W J, *Phys. Lett. B* **387** (1996) 419.
- [28] Golec-Biernat K and Wüsthoff M, *Phys. Rev. D* **59** (1999) 014017, **60** (1999) 114023.
- [29] Bartels J and Kowalski H, *Eur. Phys. J. C* **19** (2001) 93 [hep-ph/0010345].
- [30] H1 Collab., Adloff C *et al*, *Phys. Lett. B* **520** (2001) 183.
- [31] H1 Collab., Aid S *et al*, *Nucl. Phys. B* **470** (1996) 4; ZEUS Collab. Derrick M *et al*, *Z. Phys. C* **72** (1996) 399; H1 Collab., Adloff C *et al*, *Nucl. Phys. B* **497** (1997) 3; ZEUS Collab., Breitweg J *et al*, *Phys. Lett. B* **407** (1997) 432; ZEUS Collab., Breitweg J *et al*, *Eur. Phys. J. C* **7** (1999) 609; E665 Collab., Adams M R *et al*, *Phys. Rev. D* **54** (1996) 3006; ZEUS Collab., Breitweg J *et al*, *preprint DESY 00-071* (2000).
- [32] Desgrolard P, Lengyel A and Martynov E, *Pomeron effective intercept, logarithmic derivatives of $F_2(x, Q^2)$ in DIS and Regge models* [hep-ph/0110149].
- [33] Miettinen H G, in Proc. of the IX th Rencontre de Moriond, Meribel les Allues, Vol. **1** (ed. J. Tran Thanh Van), Orsay (1974); Amaldi U and Schubert K R, *Nucl. Phys. B* **166** (1980) 301.
- [34] ZEUS Collab., Breitweg J *et al*, *Eur. Phys. J. C* **6** (1999) 603, **2** (1998) 247.
- [35] ZEUS Collab., Abstract 594, EPS2001, July 2001, Budapest, Hungary.
- [36] Clerbaux B, *Vector meson production at HERA* [hep-ph/9908519].
- [37] Mellado B, *Vector meson cross sections and trajectory determination*, Proc. Int. Europhysics Conf. on HEP, Budapest 2001.
- [38] Nikolaev N N, Zakharov B G and Zoller V R, *Phys. Lett. B* **366** (1996) 337.
- [39] Nemchik J, Nikolaev N N and Zakharov B G, *Phys. Lett. B* **341** (1994) 228.
- [40] Feinberg E L, *JETP* **29** (1955) 115; Akieser A I and Sitenko A G, *JETP* **32** (1957) 744; Good M L and Walker W D, *Phys. Rev. D* **120** (1960) 1857.
- [41] Amaldi U, Jacob M and Matthiae G, *Ann. Rev. Nucl. Sci.* **26** (1976) 385.
- [42] Kaidalov A, *Phys. Rep.* **50** (1979) 157; Goulianos K, *Phys. Rep.* **101** (1983) 169.
- [43] Goulianos K, *Diffraction in hadron-hadron collisions* [hep-ph/0011060].
- [44] Batistay M, Covelan R and Montanha J, *Regge analysis of diffractive and Leading Baryon*

- structure functions from DIS [[hep-ph/0006118](#)].
- [45] Albrow M G *et al*, *Nucl. Phys.* B **51** (1973) 388; **72** (1974) 376.
- [46] Melissinos A C and Olsen S C, *Phys. Rep.* **17** (1975) 77.
- [47] see e.g. Le Bellac M, *Short-range order and local conservation of quantum numbers in multiparticle production*, CERN Yellow Report 76-14; *Acta Phys. Pol.* B **4** (1973) 901.
- [48] ZEUS Collab., Derrick M *et al*, *Phys. Lett.* B **315** (1993) 481; H1 Collab., Ahmed T *et al*, *Nucl. Phys.* B **429** (1994) 477.
- [49] Bjorken J D, AIP Conf. Proc. No.6, eds. M. Bander *et al* (AIP, New York, 1972) p. 151; Bjorken J D, Kogut J B and Soper D E, *Phys. Rev.* D **3** (1971) 1382; Bjorken J D and Kogut J B, *Phys. Rev.* D **8** (1973) 1341.
- [50] Donnachie A and Landshoff P V, *Phys. Lett.* B **191** (1987) 309.
- [51] Monaco V, *Diffractive structure functions*, [[hep-ex/0106007](#)].
- [52] Iacobucci G, *Diffractive Phenomena*, [[hep-ex/0111079](#)].
- [53] H1 Collab., Adloff C *et al*, *Z. Phys.* C **76** (1997) 613.
- [54] Gotsman E *et al*, *Energy dependence of σ^{DD}/σ_{tot} in DIS*, [[hep-ph/0007261](#)].
- [55] Batista M and Covolan R, *Phys. Rev.* D **59** (1999) 054006.
- [56] Garfagnini A (for the ZEUS collab.), *Leading baryon production in ep Scattering at HERA*, talk presented at 9th International Workshop on Deep Inelastic Scattering, DIS2001, Bologna.
- [57] Dederichs K H and Faessler M A, *Phys. Lett.* B **232** (1989) 405.
- [58] Stodolsky L, *Phys. Rev. Lett.* **28** (1972) 60; Ugaz E, *Phys. Rev.* D **17** (1978) 2475; **21** (1980) 1247.
- [59] Koba Z, Nielsen H B and Olesen P, *Nucl. Phys.* B **40** (1972) 317.
- [60] Dokshitzer Yu L, *Phys. Lett.* B **305** (1993) 295.
- [61] Benecke J, Białas A and de Groot E H, *Phys. Lett.* B **57** (1975) 447; de Groot E H, *Nucl. Phys.* B **101** (1975) 95.
- [62] Van Hove L, *Phys. Lett.* **7** (1963) 69, *Nuovo Cim.* **28** (1963) 798, *Rev. Mod. Phys.* **36** (1964) 655.
- [63] Kundrať V and Lokajicek M, *High-energy elastic hadron collisions* [[hep-ph/0001047](#)].
- [64] Andersson B, *The Lund Model*, Cambridge, Cambridge University Press, 1998.
- [65] Koba Z and Namiki M, *Nucl. Phys.* B **8** (1968) 413.
- [66] Krzywicki A, *Nucl. Phys.* B **86** (1975) 296; Grassberger P *et al*, *Nucl. Phys.* B **89** (1975) 101.
- [67] Levin E, *An Introduction to Pomerons*, [[hep-ph/9808486](#)] and [[hep-ph/9710546](#)].
- [68] Pumplin J, *Phys. Rev.* D **8** (1973) 2899.
- [69] Munier S, Stásto A M and Mueller A H, *Nucl. Phys.* B **603** (2001) 427.
- [70] Mueller A H, *Small-x Physics and Parton Saturation in QCD* [[hep-ph/9911289](#)].
- [71] Feynman R P, *Photon-Hadron Interactions*, W.A. Benjamin Inc., 1972.
- [72] Gribov V N, in: *Materials of the 8th Winter School of the Leningrad Institute of Nuclear Physics 1973* (in russian); [[hep-ph/0006158](#)] (english translation).
- [73] Landau L and Pomeranchuk I Ya, *Dokl. Akad. Nauk Ser. Fiz.* **92**, (1953) 535.
- [74] Gribov V N, Ioffe B L and Pomeranchuk I Ya, *Sov. J. Nucl. Phys.* **2** (1966) 549; *Yad. Fiz.* **2** (1965) 768.
- [75] Ioffe B L, *JETP Lett.* **9** (1969) 163; *JETP Lett.* **10** (1969) 143; *Phys. Lett.* B **30** (1969) 123.
- [76] Kovchegov Y N and Strikman M, *Phys. Lett.* B **516** (2001) 314 [[hep-ph/0107015](#)].
- [77] Dokshitzer Yu L, *JETP* **73** (1977) 1216; Gribov V N and Lipatov L N, *Sov. J. Nucl. Phys.* **15** (1972) 78; Altarelli G and G. Parisi G, *Nucl. Phys.* B **126** (1997) 298.
- [78] Lipatov L N, *Sov. J. Nucl. Phys.* **23** (1976) 338; Fadin V S, Kuraev E A and Lipatov L N, *Phys. Lett.* B **60** (1975) 50; *Sov. Phys. JETP* **44** (1976) 443, **45** (1977) 199; Balitski Y Y and Lipatov L N, *Sov. J. Nucl. Phys.* **28** (1978) 822.
- [79] Polyakov A M *Sov. Phys. JETP* **32** (1971) 296, **33** (1971) 850; Orfanidis S J and Rittenberg V, *Phys. Rev.* D **10** (1974) 2892; Cohen-Tannoudji G and Ochs W, *Z. Phys.* C **39** (1988) 513; Ochs W, *Z. Phys.* C **23** (1984) 131.
- [80] De Roeck A and De Wolf E A, *Phys. Lett.* B **388** (1996) 843.

- [81] Dokshitzer Yu L, Khoze V A, Mueller A H, and S.I. Troyan, *Basics of Perturbative QCD*, Editions Frontières, 1991.
- [82] De Wolf E A, Dremin I M and Kittel W *Phys. Rep.* **270** (1996) 1.
- [83] Mueller A H, *Phys. Rev. D* **4** (1971) 150.
- [84] Bialas A and Peschanski R, *Phys. Lett. B* **378** (1996) 302.
- [85] Miettinen H and Pumplin J, *Phys. Rev. D* **18** (1978) 1696.
- [86] Smalska B, *Diffractive results from the ZEUS LPS at HERA*, talk at DIS2001, Bologna.
- [87] Nikolaev N N and Zakharov B G, *Z. Phys. C* **49** (1990) 607; **64** (1994) 631 [[hep-ph/9306230](#)].
- [88] Forshaw J R and Ross D A, *QCD and the Pomeron*, Cambridge University Press, 1996.
- [89] Dremin I M, Gary J W, *Phys. Lett. B* **459** (1999) 341.
- [90] Frankfurt L, Miller G A and Strikman M, *Phys. Lett. B* **304** (1993) 1 [[hep-ph/9305228](#)].
- [91] Acton P D, *Z. Phys. C* **53** (1992) 539.
- [92] Capella A, *et al*, *Phys. Rev. D* **61** (2000) 074009.
- [93] Eden P, *Eur. Phys. J. C* **19** (2001) 493.
- [94] Dremin I M, Gary J W, *Phys. Rep.* **349** (2001) 301.
- [95] K. Golec-Biernat K, Motyka K and Staśto A M, *Diffusion into infra-red and unitarization of the BFKL pomeron* [[hep-ph/0110325](#)].
- [96] Golec-Biernat K, these proceedings [[hep-ph/0109010](#)].
- [97] Gribov L V, Levin E M and Ryskin M G, *Phys. Rep.* **C** 100 (1983) 1.
- [98] Staśto A M, Golec-Biernat K and Kwieciński J, *Phys. Rev. Lett.* **86** (2001) 596.
- [99] McLerran L, *Three lectures on the physics of small x and high gluon density* [[hep-ph/9903536](#)].
- [100] Berera A and Soper D E, *Phys. Rev. D* **50** (1994) 4328, *Phys. Rev. D* **53** (1996) 6162; Grazzini M, Trentadue L and Veneziano G, *Nucl. Phys. B* **519** (1998) 394; Collins J C, *Phys. Rev. D* **57** (1998) 3051.